

ELECTRON-POSITRON FLOWS AROUND MAGNETARS

ANDREI M. BELOBORODOV

Physics Department and Columbia Astrophysics Laboratory, Columbia University, 538 West 120th Street New York, NY 10027;
amb@phys.columbia.edu

Draft version October 18, 2018

ABSTRACT

The twisted magnetospheres of magnetars must sustain a persistent flow of electron-positron plasma. The flow dynamics is controlled by the radiation field around the hot neutron star. The problem of plasma motion in the self-consistent radiation field is solved using the method of virtual beams. The plasma and radiation exchange momentum via resonant scattering and self-organize into the “radiatively locked” outflow with a well-defined, decreasing Lorentz factor. There is an extended zone around the magnetar where the plasma flow is ultra-relativistic; its Lorentz factor is self-regulated so that it can marginally scatter thermal photons. The flow becomes slow and opaque in an outer equatorial zone, where the decelerated plasma accumulates and annihilates; this region serves as a reflector for the thermal photons emitted by the neutron star. The e^\pm flow carries electric current, which is sustained by a moderate induced electric field. The electric field maintains a separation between the electron and positron velocities, against the will of the radiation field. The two-stream instability is then inevitable, and the induced turbulence can generate low-frequency emission. In particular, radio emission may escape around the magnetic dipole axis of the star. Most of the flow energy is converted to hard X-ray emission, which is examined in the accompanying paper.

Subject headings: plasmas — stars: magnetic fields, neutron — X-rays

1. INTRODUCTION

The observed activity of magnetars is believed to be caused by their surface motions, which are driven by strong internal stresses. The magnetosphere is anchored in the neutron star and twisted by the surface motions, resembling the behavior of the solar corona. As a result it becomes non-potential, $\nabla \times \mathbf{B} \neq 0$, and threaded by electric currents (Thompson et al. 2002; Beloborodov & Thompson 2007). The currents flow along \mathbf{B} , i.e., the twisted magnetosphere remains nearly force-free, $\mathbf{j} \times \mathbf{B} = 0$. Numerical models of dynamic twisted magnetospheres of magnetars (Parfrey et al. 2012, 2013) show how the twist creates spindown anomalies and initiates giant flares when the magnetosphere is “overtwisted” and loses equilibrium.

Free energy stored in the magnetospheric twist is gradually dissipated through the continual electron-positron discharge that sustains the electric current. As a result, the magnetosphere tends to “untwist” on the characteristic ohmic timescale of a few years. Electrodynamics of untwisting is quite peculiar: whenever the crustal motions stop or slow down, the electric currents tend to be quickly removed from the magnetospheric field lines with small apex radii R_{\max} (Beloborodov 2009). Currents have longest lifetimes on field lines with $R_{\max} \gg R$ (where $R \approx 10$ km is the star radius) and form an extended “j-bundle” (Figure 1). The j-bundle has a sharp boundary, which gradually shrinks toward the magnetic dipole axis. In particular, the footprint of the j-bundle on the neutron star surface, which may be observed as a hot spot, shrinks with time. Shrinking hot spots were indeed reported in “transient magnetars” whose magnetospheres were temporarily activated and then gradually relaxed back to the quiescent state (see Figure 5 in Beloborodov 2011a and refs. therein).

The j-bundle must be filled with relativistic plasma

that carries the electric current $\mathbf{j} = (4\pi/c)\nabla \times \mathbf{B}$. The plasma is continually created by e^\pm discharge near the star and must expand along the extended field lines. The plasma emits persistent nonthermal emission, converting the dissipated twist energy to radiation. In the accompanying paper (Beloborodov 2013), we calculate the spectrum of produced radiation and show that it forms the observed hard X-ray component with a peak around 1 MeV. The present paper studies in more detail the dynamics of the e^\pm plasma.

Previously, semi-transparent plasma flows around magnetars were invoked to explain the deviation of the observed 1-10 keV emission from a thermal spectrum (Thompson et al. 2002). It was usually assumed that the magnetar corona is filled with positive and negative charges that are counter-streaming with mildly relativistic speeds. The counter-streaming picture was motivated by the fact that electric current \mathbf{j} must flow along the twisted magnetic field lines. The coronal plasma must be nearly neutral; it can easily carry the required current if the opposite charges with densities $n_+ = n_-$ flow in the opposite directions, so that $j = e(v_+n_+ - v_-n_-)$ where $v_+v_- < 0$. The velocities v_\pm are free parameters in this phenomenological model, which may be adjusted so that resonant scattering of thermal X-rays in the corona reproduces the 1-10 keV part of the magnetar spectrum (e.g. Fernández & Thompson 2007; Nobili et al. 2008; Rea et al. 2008).

The counter-streaming model has, however, a problem. Note that the thermal radiation of the magnetar ($h\nu \sim 1$ keV) is resonantly scattered at large radii $r \sim 10R \approx 100$ km where $B \sim 10^{11} - 10^{12}$ G.¹ In this region, the plasma is strongly pushed by radiation away from the star and the counter-streaming model needs an

¹ This assumes that photons are scattered by electrons, not ions.

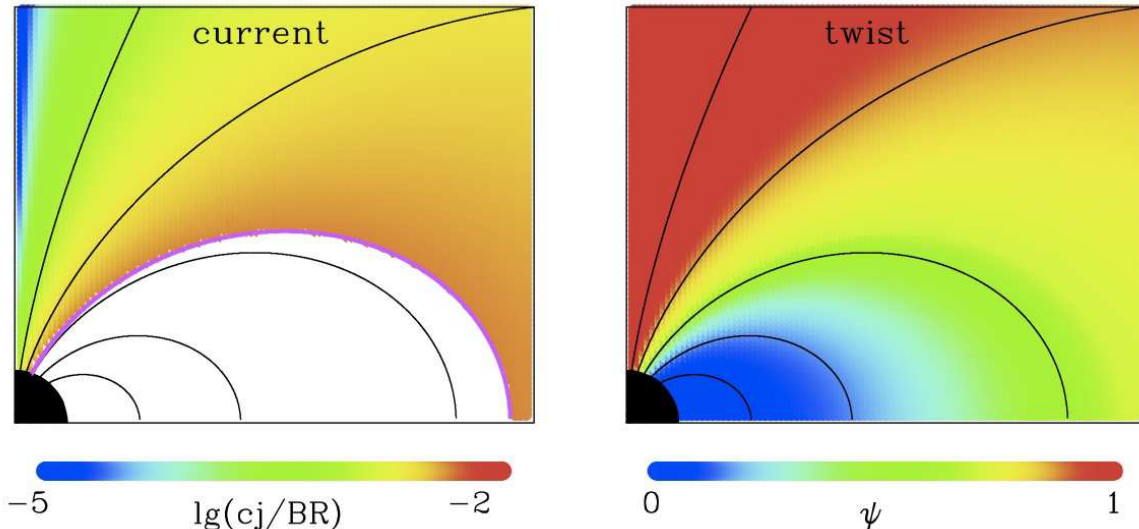


FIG. 1.— Snapshot of a slowly untwisting magnetosphere. In this example, a global twist with a uniform amplitude $\psi = 0.2$ was implanted into the dipole magnetosphere at $t = 0$, and the snapshot shows the magnetosphere at $t \sim 1$ yr. Details of the calculations are described in Beloborodov (2009). The plane of the figure is the poloidal cross section of the magnetosphere. The black curves are the poloidal magnetic field lines. The magnetosphere is symmetric about the vertical axis and the equatorial plane; therefore, the figure only shows one quarter of the poloidal cross section. The neutron star is shown by the black circle (radius $R \approx 10$ km). Left panel: Current density j normalized to BR/c . The region from which currents have been pulled into the star (the potential “cavity” with $j = 0$) is shown in white. The boundary between the cavity and the j -bundle (magenta curve) expands with time, i.e. the j -bundle shrinks toward the vertical axis. Right panel: Twist amplitude ψ at the same time. The twist amplitude is defined for each closed field line as the azimuthal displacement of its footpoint in the southern hemisphere relative to the footpoint in the northern hemisphere.

electric field E_{\parallel} that forces charges of the right sign to move toward the star against the radiative drag. At the same time, the electric field acts on the opposite charges and accelerates them away from the star, cooperating with the radiative push. In the presence of e^{\pm} plasma (which is inevitably created near magnetars), the outward acceleration generates relativistic particles, and no self-consistent solution exists for the mildly-relativistic counter-streaming model.

In this paper (and the accompanying paper Beloborodov (2013)), we develop a different picture of plasma circulation in the magnetar corona. It is schematically shown in Figure 2. The outer corona is inevitably filled with e^{\pm} pair plasma of a high density n , which is larger than j/ec by the “multiplicity factor” $\mathcal{M} \gg 1$; in this respect it resembles the flow along the open field lines of a rapidly rotating, strongly magnetized neutron star (e.g. Hirschman & Arons 2001; Thompson 2008a; Medin & Lai 2010). Pairs are created in the “adiabatic zone” $B > 10^{13}$ G where the flow energy is reprocessed into particles with Lorentz factors $\gamma \sim 20$ (Beloborodov 2013); their multiplicity $\mathcal{M} \sim 10^2$ is basically set by energy conservation and mainly controlled by the discharge voltage. Both electrons and positrons outflow from the magnetar, and radiation pressure forces the particles to accumulate in the equatorial plane of the magnetic dipole, where they annihilate. The required current $\mathbf{j} = (c/4\pi)\nabla \times \mathbf{B}$ is sustained in the outflow by a moderate electric field E_{\parallel} . This field is self-consistently generated to maintain a small difference between the velocities of the \pm charges, $(v_+ - v_-)/v_{\pm} \sim \mathcal{M}^{-1} \ll 1$, so that the condition $e(n_+v_+ - n_-v_-) = j$ is satisfied with $n_+ \approx n_-$ and $v_+v_- > 0$. In the simplest, two-fluid model (Section 3) the velocities v_{\pm} tend to be “locked” by the balance of two forces, electric and radiative.

The coronal outflow significantly changes the radiation it interacts with via scattering. The problem of outflow dynamics can be formulated as a problem of self-consistent radiative transfer where particles and photons exchange energy and momentum as they flow away from the neutron star. This problem is solved in this paper using a specially designed numerical method.

The paper is organized as follows. Section 2 discusses the creation of e^{\pm} pairs and their circulation in the inner and outer magnetosphere. Section 3 presents the model of a radiatively locked outflow in its simplest version using a two-fluid description and assuming an optically thin magnetosphere. Section 4 discusses the two-stream instability in the e^{\pm} flow and the origin of low-frequency emission from magnetars. Then, in Sections 5 and 6 we formulate and solve the full problem where an outflow with a broad momentum distribution function and significant optical depth interacts with the neutron-star radiation. The numerical method and results are described in Section 6. Our conclusions are summarized in Section 7.

2. CREATION AND CIRCULATION OF E^{\pm} PAIRS

The creation of e^{\pm} pairs by an accelerated particle is a two-step process: the particle generates a high-energy photon (via resonance scattering) and then the photon converts to an e^{\pm} pair in the strong magnetic field. An accelerated electron (or positron) can resonantly scatter photons of energy $\hbar\omega$ once it reaches the Lorentz factor required by the resonance condition $\gamma(1 - \beta \cos \vartheta)\omega = \omega_B$, where ϑ is the angle between the photon and the electron velocity and $\omega_B = eB/m_e c$. When ϑ is not small, the resonance condition gives

$$\gamma_{sc} \sim 10^3 B_{14} \left(\frac{\hbar\omega}{1 \text{ keV}} \right)^{-1}. \quad (1)$$

The scattered photons are boosted in energy by the factor of $\sim \gamma_{sc}^2$. Such high-energy photons quickly convert to e^\pm pairs in the strong magnetic field, creating more particles near the star. A similar process of e^\pm creation operates in the polar-cap discharge of ordinary pulsars, but in a different mode. In ordinary pulsars, the high-energy photons convert to e^\pm with a significant delay. The scattered photon initially moves nearly parallel to \mathbf{B} and converts to e^\pm only when it propagates a sufficient distance where its angle θ_γ with respect to \mathbf{B} increases so that the threshold condition for conversion is satisfied. This delay leads to the large unscreened voltage in pulsar models.

In contrast, the magnetic field of magnetars is so strong that pair creation can occur immediately following resonant scattering (Beloborodov & Thompson 2007). The energy of a resonantly scattered photon is related to its emission angle θ_γ by

$$E(\theta_\gamma) = \frac{E_B}{\sin^2 \theta_\gamma} \left[1 - \left(\cos^2 \theta_\gamma + \frac{m_e^2 c^4}{E_B^2} \sin^2 \theta_\gamma \right)^{1/2} \right], \quad (2)$$

where $E_B = (2B/B_Q + 1)^{1/2} m_e c^2$ is the energy of the first excited Landau level and $B_Q = m_e^2 c^3 / \hbar e \approx 4.4 \times 10^{13}$ G. The scattered photon may immediately be above the threshold for conversion, $E > E_{thr} = 2m_e c^2 / \sin \theta_\gamma$, if $B > 4B_Q$. Therefore, e^\pm discharge in magnetars can screen E_\parallel more efficiently than in ordinary pulsars and buffer the voltage growth once the Lorentz factors of accelerated particles reach γ_{sc} given in Equation (1).

2.1. Pair creation on field lines with apices

$$R_{max} \lesssim 2R$$

The discharge on twisted closed field lines can be explored using a direct numerical experiment where plasma is represented by a large number of individual particles in the self-consistent electric field. The existing numerical simulations (Beloborodov & Thompson 2007) describe the discharge on field lines that extend to a moderate radius $R_{max} \lesssim 2R$, where R is the radius of the neutron star. The magnetic field is ultrastrong everywhere along such field lines, $B \gg B_Q$, and resonant scattering events may effectively be treated as events of pair creation — a significant fraction of scattered photons immediately convert to e^\pm .

The simulations demonstrate that voltage and pair creation self-organize in the twisted magnetosphere so that a particle on average scatters ~ 1 photon as it travels through the electric circuit, maintaining the near-critical multiplicity of pair creation $\mathcal{M} \sim 1$. This criticality condition regulates the induced voltage to $\Phi_e \sim 10^9$ V, which accelerates e^\pm particles to Lorentz factors $\gamma \sim 10^3$. The electric circuit operates as a *global* discharge, in the sense that the accelerating voltage is distributed along the entire field line between its footpoints on the star. It is quite different from the localized “gap” that is usually considered above polar caps in pulsars.

The discharge fluctuates on the light-crossing timescale $\sim R/c$ and persists in the state of self-organized criticality. The behavior of the global circuit resembles a continually repeating lightning: voltage between the footpoints of the field line quasi-periodically builds up and discharges through the enhanced production of charges.

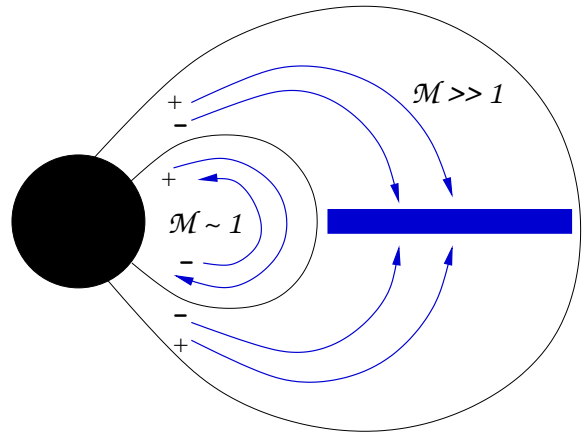


FIG. 2.— Schematic picture of plasma circulation in the magnetosphere with surface $B \sim 10^{15}$ G. Two regions are indicated. (1) “Inner corona.” Here e^\pm have a moderate multiplicity $\mathcal{M} \sim 1$. The particles do not stop in the equatorial plane. The electric field E_\parallel ensures that electrons and positrons circulate in the opposite directions along the magnetic field lines, maintaining the electric current demanded by $\nabla \times \mathbf{B}$. The particles are lost as they reach the footpoints of the field line and continually replenished with pair creation. (2) “Outer corona” — extended field lines with $R_{max} \gg R$. Electrons and positrons are created by the discharge near the star and some of them flow outward to the region of weaker B . Here resonant scattering enhances the pair multiplicity, $\mathcal{M} \gg 1$, and decelerates the outflow. The e^\pm particles stop at the apices of magnetic field lines (blue region in the equatorial plane), accumulate, and annihilate there. The number fluxes of electrons and positrons toward the annihilation region differ by a small fraction $\sim \mathcal{M}^{-1}$, so that the outflow carries the required electric current $\mathbf{j} = (c/4\pi)\nabla \times \mathbf{B}$. Electrodynamics of the twist dissipation implies that the inner corona is less likely to be active, as the electric currents are erased by the expanding cavity (Figure 1); the observed activity tends to concentrate on extended field lines that form the outer corona.

The average plasma density in the circuit n is close to the minimum density $n_{min} = j/ec$, as required by the criticality condition $\mathcal{M} = n/n_{min} \sim 1$.

The global-discharge picture applies only to field lines with $R_{max} \lesssim 2R$ and becomes irrelevant when the currents are erased in the inner magnetosphere as shown in Figure 1. Then the observed activity must be associated with currents on field lines with large R_{max} , i.e. extending far from the star.

2.2. Pair creation on field lines with apices $R_{max} \gg R$

The discharge on extended field lines may be expected to have a similar threshold voltage $\Phi_e \sim 10^9$ V, because the conversion of upscattered photons to e^\pm is efficient near the field-line footpoints where $B \gg B_Q$. In this zone, particles are able to resonantly scatter soft X-rays once they are accelerated to $\gamma \sim 10^3$ (Equation 1), which requires $\Phi_e \sim 10^9$ V. Further growth of voltage would cause excessive creation of e^\pm moving in both directions, toward and away from the star, leading to efficient screening of E_\parallel .

A large fraction of the created particles must outflow to $r \gg R$ along the extended field lines. The rate of resonant scattering by a relativistic particle *increases* as it moves from $B \gg B_Q$ to $B \lesssim B_Q$. The particle scatters many more photons, because the resonance condition shifts toward photons of lower energy $\hbar\omega_{res} \propto B$ whose number density is larger. Note also that the effective

cross section for resonant scattering $\sigma_{\text{res}} = 2\pi^2 r_e c / \omega_{\text{res}}$ increases as B^{-1} (here $r_e = e^2 / m_e c^2$ is the classical electron radius). Practically all photons scattered by the outflowing particles in the region $B \gtrsim 10^{13}$ G convert to e^\pm ; detailed Monte-Carlo simulations of this process are presented in the accompanying paper (Beloborodov 2013). In essence, the particles outflowing from the discharge zone lose energy to photon scattering, and this energy is transformed to new generations of e^\pm . As a result, the e^\pm multiplicity of the outflow increases from $\mathcal{M} \sim 1$ to $\mathcal{M} \sim 100$. This implies that there is no charge starvation in the outer corona — there are plenty of charges to conduct the current demanded by the twisted magnetic field.

Pair creation sharply ends near the surface of $B \approx 10^{13}$ G; outside this surface the resonantly scattered photons are not absorbed. The steady relativistic outflow without pair creation maintains $\mathcal{M} = \text{const}$ along the magnetic field lines. This follows from conservation of magnetic flux, charge, and particle number, which give $n/B = \text{const}$, $j/B = \text{const}$, and $n/j = \text{const}$ along the field line.

2.3. Global circulation of pair plasma

The picture of plasma circulation in the magnetar magnetosphere is summarized in Figure 2. The inner corona (field lines with R_{max} of a few neutron-star radii) is filled with the ultra-relativistic counter-streaming e^- and e^+ . In this region, resonant scattering is marginally efficient and a global discharge operates as described in Section 2.1, with multiplicity $\mathcal{M} \sim 1$. Outside this region, pair multiplicity is much higher and the electric current is organized with both e^- and e^+ outflowing from the star. The exact location of the boundary between the two regions depends on the strength of the magnetic field of the star.

In the outer corona, the opposite flows in the northern and southern hemispheres meet in the equatorial plane of the magnetic dipole and stop there. Two effects prevent their inter-penetration. (1) Radiative drag is strong in the outer corona and pushes both northern and southern flows toward the equatorial plane (see Section 3 below). (2) When the two opposite flows try to penetrate each other, a two-stream instability develops. As a result, a strong Langmuir turbulence is generated, which inhibits the penetration. This effect is particularly important in the transition region between the outer and inner corona. For these field lines, resonant scattering is efficient enough to generate $\mathcal{M} > 1$ but not strong enough to stop the pair plasma in the equatorial plane. Then the colliding northern and southern flows are stopped by the two-stream instability. This behavior contrasts with the inner corona where the induced electric field enforces the counter-streaming of e^- and e^+ , i.e. the opposite flows with $\mathcal{M} \sim 1$ are forced to penetrate each other despite the two-stream instability.

The density of e^\pm pairs accumulated in the outer equatorial region (shown in blue in Fig. 2) is regulated by the annihilation balance. In a steady state, the annihilation rate is given by $\dot{N}_{\text{ann}} \approx 2\mathcal{M}(I/e)$, where I is the electric current through the annihilation region. The corresponding annihilation luminosity is $L_{\text{ann}} = 2m_e c^2 \mathcal{M} I / e$.

3. RADIATIVELY LOCKED CORONAL FLOW

Dynamics of the e^\pm flow in the outer corona ($r \gg R$) is influenced by resonant scattering, which exerts a strong force \mathcal{F} on the particles along the magnetic field lines. \mathcal{F} vanishes only if the particle has the “saturation momentum” p_\star such that the radiation flux measured in the rest frame of the particle is perpendicular to \mathbf{B} . In the simplest case of a weakly twisted dipole magnetosphere exposed to central radiation p_\star is given by (Appendix B),²

$$p_\star(r, \theta) = \frac{2 \cos \theta}{\sin \theta}, \quad (3)$$

where momentum is in units of $m_e c$. The radiative force always pushes the particle toward $p = p_\star$. The strength of this effect may be measured by the dimensionless “drag coefficient,”

$$\mathcal{D} \equiv \frac{r\mathcal{F}}{p m_e c^2}. \quad (4)$$

Momentum p_\star is a strong attractor in the sense that deviations $p - p_\star$ generate $\mathcal{D} \gg 1$ in the outer corona (see Appendix A).

Even an extremely strong radiative drag does not imply that e^+ and e^- acquire exactly equal velocities $\beta_+ = \beta_- = \beta_\star = p_\star(1 + p_\star^2)^{-1/2}$. Such a “single-fluid” flow would be unable to carry the required electric current j , and E_\parallel must be induced to ensure a sufficient velocity separation $\beta_+ - \beta_-$. Below we describe the two-fluid model with $\beta_+ \neq \beta_-$.

3.1. Two-fluid model: basic equations

Consider an e^\pm flow in the region where no new pairs are produced. In a steady state, the fluxes of electrons and positrons are conserved $\nabla \cdot (n_\pm \mathbf{v}_\pm) = 0$. This implies $\nabla \cdot \mathbf{j}_\pm = 0$ where $\mathbf{j}_\pm = \pm en_\pm v_\pm$ are the contributions of electrons and positrons to the net electric current $\mathbf{j} = \mathbf{j}_+ + \mathbf{j}_-$. Since e^\pm move along the magnetic field lines, $\mathbf{j}_\pm = \alpha_\pm \mathbf{B}$ where α_\pm are scalar functions. From $\nabla \cdot \mathbf{j}_\pm = 0$ and $\nabla \cdot \mathbf{B} = 0$ one gets $\mathbf{B} \cdot \nabla \alpha_\pm = 0$. Therefore,

$$\frac{j_+}{B} = \text{const}, \quad \frac{j_-}{B} = \text{const}, \quad (5)$$

are constant along the field line. The net current $j = j_+ + j_-$ is fixed by the condition $j = (c/4\pi)|\nabla \times \mathbf{B}|$. The multiplicity of pairs is defined by

$$\mathcal{M} = \frac{j_+ + |j_-|}{j}. \quad (6)$$

Here “+” corresponds to positrons, which carry current $j_+ > 0$ and “-” corresponds to electrons, which carry $j_- < 0$; we assume a positive net current $j = j_+ + j_-$ for definiteness. A counter-streaming model ($v_+ v_- < 0$) would have $\mathcal{M} = 1$. A charge-separated outflow ($n_- = 0$) would also have $\mathcal{M} = 1$. We study here pair-rich outflows with $\mathcal{M} > 1$.

The outflowing e^\pm plasma must be nearly neutral,³

$$n_+ \approx n_-, \quad (7)$$

² This expression is valid in the region where $1 - B_r/B > (R/r)^2$. In this region, stellar radiation may be approximated as a central flow of photons, neglecting the angular size of the star $\sim R/r$.

³ Here we neglect rotation of the neutron star and its magnetosphere, which is a good approximation everywhere except the open field-line bundle that connects the star to the light cylinder.

otherwise a huge electric field would be generated that would restore neutrality. Using this condition, one finds that $en_+v_+ - en_-v_- = j$ is satisfied if

$$1 - \frac{\beta_-}{\beta_+} = \frac{2}{\mathcal{M} + 1}. \quad (8)$$

A deviation from this condition implies a mismatch between the conduction current $j_+ + j_-$ and $(c/4\pi)\nabla \times \mathbf{B}$, which would induce a growing electric field according to Maxwell equation $\partial \mathbf{E}/\partial t = c\nabla \times \mathbf{B} - 4\pi \mathbf{j}$. An electric field E_{\parallel} must be established in the outflow to sustain the condition (8) against the radiative drag that tends to equalize β_- and β_+ at β_* . This moderate electric field must be self-consistently generated by a small deviation from neutrality, $\delta n = n_+ - n_- \ll n_{\pm}$.

The two-fluid dynamics of the outflow is governed by two equations,

$$m_e c^2 \frac{d\gamma_{\pm}}{dl} = \mathcal{F}(\gamma_{\pm}) \pm eE_{\parallel}, \quad (9)$$

where l is length measured along the magnetic field line. In the region of strong drag, $|\mathcal{D}| \gg 1$, the left-hand side is small compared with \mathcal{F} ; then the radiative and electric forces on the right-hand side nearly balance each other, $\mathcal{F}(\gamma_+) \approx -eE_{\parallel}$ and $\mathcal{F}(\gamma_-) \approx eE_{\parallel}$. This implies,

$$\mathcal{F}(\gamma_+) \approx -\mathcal{F}(\gamma_-) \quad (|\mathcal{D}| \gg 1). \quad (10)$$

Equations (8) and (10) describe the ‘‘radiatively locked’’ two-fluid current with pair multiplicity \mathcal{M} . The solution γ_{\pm} to these equations exists if $\mathcal{M} > 1$. Note that $\beta_- < \beta_* < \beta_+$ in the radiatively-locked state.

Let us now relax the assumption $|\mathcal{D}| \gg 1$. Then the inertial term $m_e c^2 d\gamma_{\pm}/dl$ must be retained in Equations (9), i.e. we now deal with differential equations for γ_{\pm} . Since γ_- and γ_+ are not independent — they are related by condition (8) — it is sufficient to solve one dynamic equation, e.g. for γ_+ (and use the dynamic equation for γ_- to exclude E_{\parallel}). Straightforward algebra gives,

$$m_e c^2 \frac{d\gamma_+}{dl} = \frac{\mathcal{F}(\gamma_+) + \mathcal{F}(\gamma_-)}{1 + d\gamma_-/d\gamma_+}, \quad (11)$$

$$\frac{d\gamma_-}{d\gamma_+} = \left(\frac{\mathcal{M} - 1}{\mathcal{M} + 1} \right)^2 \left(\frac{\gamma_-}{\gamma_+} \right)^3. \quad (12)$$

3.2. Sample numerical model

Suppose that e^{\pm} plasma is injected near the star with a given multiplicity, e.g. $\mathcal{M} = 50$, and a given high Lorentz factor, e.g. $\gamma_+ = 100$. The corresponding γ_- is determined by Equation (8). Suppose that the plasma is illuminated by the blackbody radiation of the star of temperature $kT = 0.5$ keV and neglect radiation from the magnetosphere itself. This approximation is valid

der. In a more exact model, the Gauss law in the co-rotating frame $\nabla \cdot \mathbf{E} = 4\pi(\rho + \rho_v)$ includes the effective vacuum charge density $\rho_v = \mathbf{\Omega} \cdot \mathbf{B}/2\pi c$ where $\mathbf{\Omega}$ is the angular velocity of the star (Goldreich & Julian 1969). Then the neutrality condition becomes $e(n_+ - n_-) + \rho_v = 0$. Magnetars rotate slowly (typical $\Omega \sim 1$ rad/s) and hence a small fraction of their magnetic flux is open, typically $\lesssim 10^{-4}$. In the main, closed magnetosphere, the condition $|\rho_v/e| \ll |j/ec| < n_{\pm}$ is satisfied, and neutrality requires $n_+ \approx n_-$ with a high accuracy.

only for optically thin magnetospheres, which are considered here for simplicity. A more detailed model will be developed in Sections 5 and 6, which will take into account radiation scattered in the magnetosphere; then radiation field is not central, and we will have to solve radiative transfer to determine the flow momentum.

An explicit expression for $\mathcal{F}(\gamma)$ exerted by the central radiation is given in Appendix B (Equation B6). The steady-state solution for γ_{\pm} in the outer corona can be found by integrating Equation (11) along the magnetic field lines. The result is shown in Figure 3. The relativistic outflow is injected near the star and initially weakly interacts with the radiation; then it enters the drag-dominated region $|\mathcal{D}| \gg 1$. The solution is not sensitive to the precise radius of e^{\pm} injection as long as it is small enough, before the plasma enters the drag-dominated region.

The electric field in the region of $|\mathcal{D}| \gg 1$ is given by $eE_{\parallel} \approx -\mathcal{F}(\gamma_+)$, and the corresponding longitudinal voltage established in the outer corona is found by integrating $\mathcal{F}(\gamma_+)$ along the field line, $e\Phi_e \approx -\int \mathcal{F}(\gamma_+) dl$. Its typical value for the model in Figure 3 is $\sim 10^7$ V. Flows with lower \mathcal{M} develop stronger electric fields, however in all cases of interest ($\mathcal{M} \gg 1$) the drag-induced voltage is below 10^9 V.

The calculations shown in Figure 3 assume that the magnetospheric plasma is everywhere optically thin. This is not so for real magnetars. Thompson et al. (2002) showed that the characteristic optical depth τ of a strongly twisted magnetosphere (twist amplitude $\psi \sim 1$) is comparable to unity. When the large pair multiplicity \mathcal{M} is taken into account, the estimate changes to

$$\tau \sim \frac{\mathcal{M}\psi}{\beta_{\pm}} \gg 1. \quad (13)$$

This estimate describes the optical depth seen by photons that can be resonantly scattered by the flow, i.e. the resonance condition $\gamma(1 - \beta \cos \vartheta)\omega = \omega_B$ is satisfied somewhere along the photon trajectory. The large τ implies the presence of scattered radiation in the magnetosphere, which is quasi-isotropic rather than central. This increases the drag exerted on the outflow and reduces p_* . One may also expect a self-shielding effect: the drag force \mathcal{F} experienced by an electron (or positron) is reduced by the factor of τ^{-1} . The problem of self-consistent outflow dynamics will be solved in Sections 5 and 6. The main feature seen in Figure 3 will persist in the full self-consistent solution: the outflow is strongly decelerated (and drag-dominated) in the equatorial region at $r \sim (10 - 20)R$.

4. TWO-STREAM INSTABILITY, ANOMALOUS RESISTIVITY, AND RADIO EMISSION

4.1. Two-stream instability

The two-fluid flow with $v_+ > v_-$ is prone to the two-stream instability (e.g. Krall & Trivelpiece 1973). The growth rate of the instability is obtained from the dispersion relation for Langmuir modes with frequency ω and wavevector k , which can be derived by considering perturbations $\delta\gamma_{\pm}$ of the two-fluid system and using con-

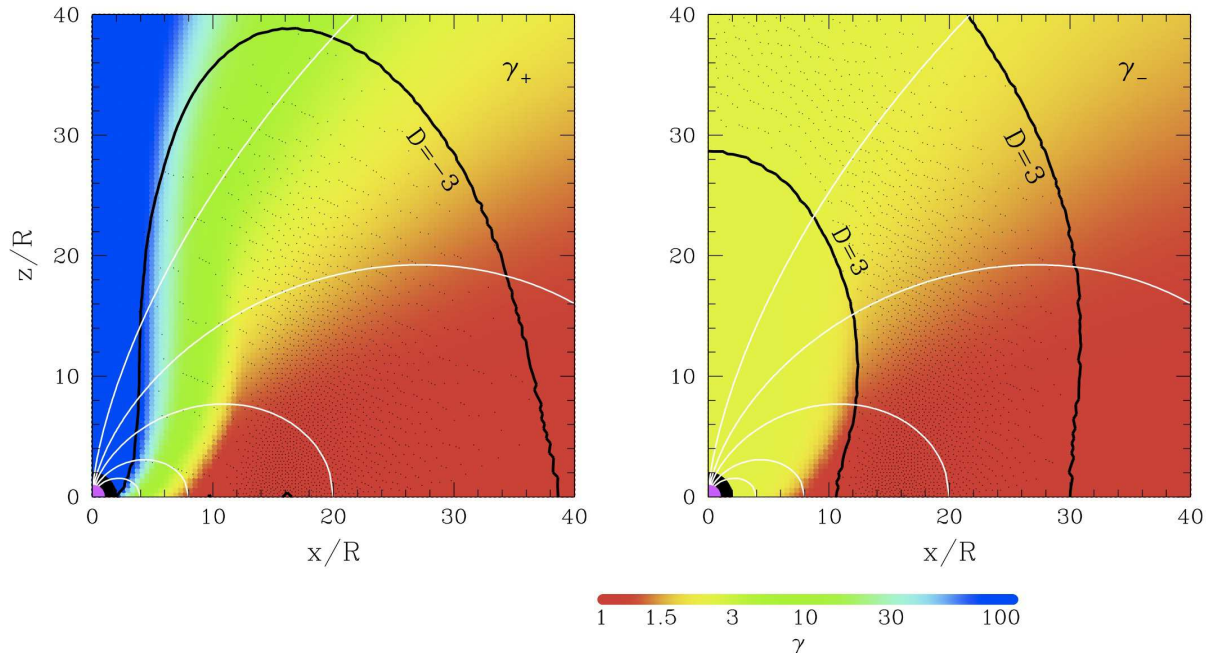


FIG. 3.— Lorentz factors γ_+ (left panel) and γ_- (right panel) in the two-fluid model of the e^\pm flow. In this example, the electric current is carried by the e^\pm outflow of a fixed multiplicity $\mathcal{M} = 50$. The plasma is injected at radius $r = 2R$ and outflows along the magnetic field lines (white curves). The flow is illuminated by the star with temperature $kT = 0.5$ keV (magenta circle at the origin), and the radiation exerts the forces $\mathcal{F}(\gamma_\pm)$ on the positron (+) and electron (−) fluids. The Lorentz factors γ_+ and γ_- change as the flow enters the drag-dominated region $|\mathcal{D}| \gg 1$. The region $|\mathcal{D}| > 3$ is shown by the thick black curve and shadowed in black. $\mathcal{D} < 0$ for positrons ($\gamma_+ > \gamma_*$) and $\mathcal{D} > 0$ for electrons ($\gamma_- < \gamma_*$). The radiative drag stops the plasma in the equatorial plane outside $\sim 8R$. A nearly dipole magnetic field (weakly twisted) with $B_{\text{pole}} = 10^{15}$ G is assumed in this example. R is the neutron-star radius.

tinuity, Euler, and Poisson equations,

$$1 - \frac{\omega_+^2}{\gamma_+^3(\omega - kv_+)^2} - \frac{\omega_-^2}{\gamma_-^3(\omega - kv_-)^2} = 0, \quad (14)$$

where $\omega_\pm^2 = 4\pi n_\pm e^2/m_e$. The plasma is nearly neutral, $n_+ = n_-$, and hence $\omega_+ = \omega_-$. Equation (14) has a solution $\omega(k)$ with a positive imaginary part that describes an unstable mode. The solution simplifies in the following two limits:

(1) $\gamma_+ - \gamma_- \ll \gamma_\pm$, which is valid when $\mathcal{M} \gg \gamma_\pm^2$ (see Equation 8). Then the flow is convenient to view in its center-of-momentum frame that moves with $v \approx (\gamma_+ + \gamma_-)/2$. In this frame, the two fluids with densities $\tilde{n}_\pm = \gamma^{-1}n_\pm$ move in the opposite directions with non-relativistic velocities $\tilde{v}_\pm = \pm\tilde{v}$, so the dispersion relation (14) simplifies. It gives the most unstable mode $\tilde{k} = (\sqrt{3}/2)\tilde{\omega}_\pm/\tilde{v}$ with a growth rate $\tilde{\Gamma} = \tilde{\omega}_\pm/2$.

(2) $\gamma_+/\gamma_- \gg 1$. Then the contribution of positrons to the dispersion relation is small compared to that of the electrons. The growth rate of the instability is given by $\Gamma \approx \gamma_-^{-1/2}\gamma_+^{-1}\omega_p$ (e.g. Lyubarsky & Petrova 2000).

This estimate gives the characteristic length-scale of the instability c/Γ , which is much shorter than the electron free path to resonant scattering, λ_{sc} . Hence the radiation drag and the induced electric field $eE_\parallel = \pm\mathcal{F}(p_\pm)$ are unable to lock the positive and negative charges at the momenta p_+ and p_- calculated in the two-fluid model. The instability will generate plasma oscillations that should broaden the momentum distribution so that particles fill the region $p_- < p < p_+$.

The generated plasma oscillations may be expected to

introduce an anomalous resistivity. The fluctuating E_\parallel in the oscillations creates a stochastic force that tends to reduce the free-path of a charged particle. A simplest estimate suggests that this effect could be very strong. Suppose a substantial fraction of the energy density of the flow $\gamma m_e c^2 n$ is given to plasma oscillations. Then the characteristic electric field is $E_\parallel \sim (8\pi\gamma m_e c^2 n)^{1/2}$; it is much stronger than E_\parallel in the radiatively locked two-fluid model, however it is irregular and quickly changes sign. Suppose that the stochastic electric force exerted on the particle randomly changes sign on a timescale $\Delta t \sim \omega_p^{-1}$, where ω_p is the plasma frequency. The stochastic E_\parallel gives the momentum kicks $\Delta P \sim eE_\parallel\omega_p^{-1}$ and causes diffusion of particles in the momentum space with the diffusion coefficient

$$D_p \sim \frac{(\Delta P)^2}{\Delta t} \sim \frac{(eE_\parallel)^2}{\omega_p}. \quad (15)$$

Diffusion in momentum space $p^2(t) \sim D_p t$ implies a small free-path of the particle, $\lambda \sim (\gamma\beta)^2 m_e^2 c^3 \omega_p / (eE_\parallel)^2$, much smaller than the mean free path to resonant scattering. Thus, a large anomalous resistivity could, in principle, be possible, and then a large longitudinal voltage would be generated to maintain the electric current.

4.2. Numerical experiment

To explore the role of the two-stream instability and anomalous resistivity, we designed the following numerical experiment. Keeping in mind that particles around magnetars can flow only along the magnetic field lines, consider the simple one-dimensional problem. Suppose

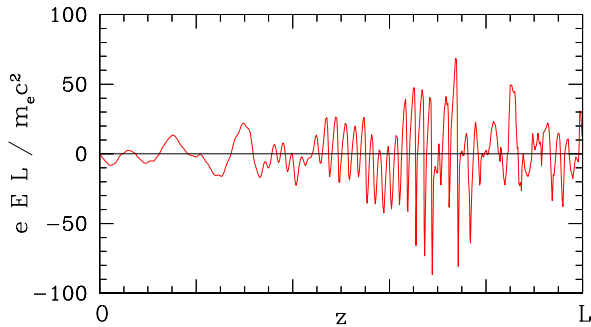


FIG. 4.— Snapshot of electric field in the simulation box.

an e^\pm beam is continually injected at the boundary $z = 0$ of the computational box $0 < z < L$. The rate of electron injection is smaller than the rate of positron injection, so that the flow carries current $j > 0$. Positrons are injected with fixed p_+ and electrons with fixed $p_- < p_+$; we chose $p_+ = 7$ and $p_- = 0.5$. The simulation keeps track of the flow in the computational box of length $L \sim 150c/\omega_p$. The escape boundary condition is implemented at $z = L$. The flow is simulated as a large collection of individual particles ($N \sim 10^6$) that move in their collective electric field (see Beloborodov & Thompson [2007] for details of the numerical method). The simulation was run for a time of $t \sim 100L/c$, long enough to see the quasi-steady behavior.

The results of the simulation are as follows. As expected, strong plasma oscillations develop and persist in the flow, as the instability is continually fed by the injection of the two streams at $z = 0$. The fluctuating electric field reaches very high amplitudes that could reverse a particle with Lorentz factor γ_+ on a short scale, much shorter than L . A snapshot of $E_{\parallel}(z)$ is shown in Figure 4. The integral of the electric field over z determines the voltage Φ_e between the two boundaries of the computational box. The measured Φ_e in the simulation fluctuates in time (Figure 5), and we calculated its value averaged over $100L/c$. This value turns out to be very small, $e\Phi_e \sim 0.1\gamma_+m_e c^2$. Thus, the measured anomalous resistivity is small, in sharp contrast with the simplest estimate (15) that would predict $\lambda \ll L$ and hence $e\Phi_e \gg \gamma_+m_e c^2$.

The failure of the estimate (15) is related to the assumption that the stochastic electric force applied to the particle is random, uncorrelated on timescales longer than ω_p^{-1} . The numerical simulation indicates that this assumption is incorrect. Apparently, a complicated time-dependent pattern is organized in the phase space, which allows the charges to find small-resistance paths through the waves of E_{\parallel} and conduct the current at a low net voltage and a low dissipation rate.

One limitation of the numerical experiment should be noted: the one-dimensional computational box allows no dependence of E_{\parallel} on the transverse coordinates x and y , which excludes the coupling of Langmuir waves to the transverse electro-magnetic modes. A two-dimensional (or a complete three-dimensional) simulation will be needed to explore the role of the transverse modes. We anticipate that a low anomalous resistivity will be found

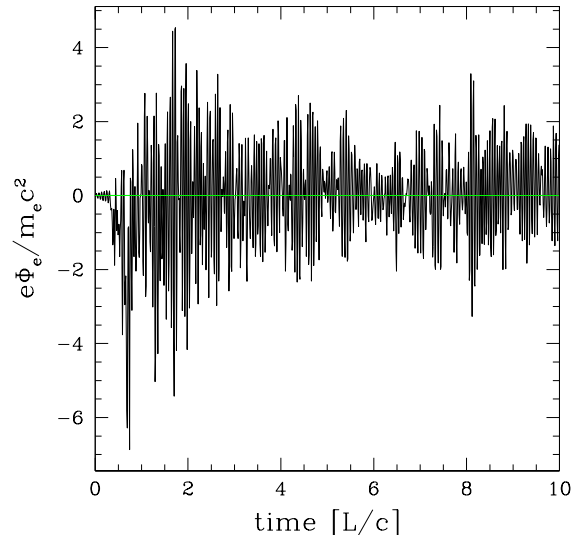


FIG. 5.— Voltage across the simulation box as a function of time.

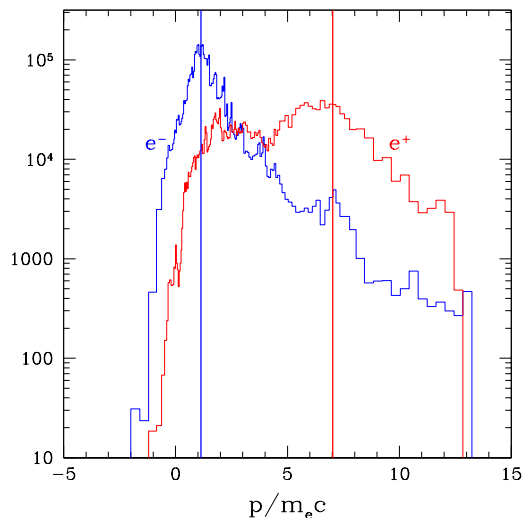


FIG. 6.— Snapshot of the momentum distributions of e^+ (red) and e^- (blue). Vertical lines show the injection p_{\pm} at $z = 0$.

in the full simulations. A high resistivity would imply a quick dissipation of magnetospheric currents, which would produce a high luminosity and quickly erase the magnetic twist. This is not supported by observations of magnetars. The observed luminosities and evolution timescales are consistent with the model neglecting the anomalous resistivity, where voltage is controlled by the threshold of the e^\pm discharge, $e\Phi_e \sim 10^9 - 10^{10}$ V.

The numerical simulation shows that the two-stream instability significantly changes the momentum distributions of electrons and positrons from the injected delta-functions $\delta(p - p_-)$ and $\delta(p - p_+)$. The e^\pm distributions are broadened so that they fill the region between the injection momenta p_+ and p_- (Figure 6).

4.3. Low-frequency emission

An important implication of the two-stream instability is the excitation of a strong plasma turbulence that can generate coherent low-frequency radiation. The two-stream instability is often considered in pulsar models as a mechanism feeding radio emission from the open field-line bundle (e.g. Sturrock 1971; Cheng & Ruderman 1977). A related model invoking radiative drag was considered by Lyubarsky & Petrova (2000).⁴ In the e^\pm flows around magnetars, the two stream instability is naturally driven by the strong electric current in the system that tends to lock itself in the two-fluid configuration as described in Section 3. The instability is continually pumped by the radiative drag in the dense radiation field of the magnetar. The generated low-frequency radiation has the best chance to escape near the magnetic axis, where the plasma density is lowest and its Lorentz factor is highest. Note that the two-stream instability operates on the closed (twisted) field lines, which carry significant magnetic flux. This allows the low-frequency emission to be unusually bright, even though the voltage $\Phi_e \sim 10^9 - 10^{10}$ V is small by the ordinary-pulsar standards.

Radio pulsations have been detected and studied in detail in two magnetars XTE 1810-197 and 1E 1547.0-5408 (Camilo et al. 2006; 2007). The estimated radio luminosity $L_r \sim 10^{30}$ erg s⁻¹ requires a sufficiently high ohmic dissipation rate, $I\Phi_e > L_r$, which cannot be generated in the open field-line bundle unless Φ_e exceeds $L_r/I_{LC} \sim 10^{11}\varepsilon_r^{-1}L_{r,30}$ V. Here ε_r is the efficiency of radio emission, I_{LC} is the electric current circulating in the open bundle, $I_{LC} \sim c\hat{\mu}/R_{LC}^2$, and $R_{LC} = cP/2\pi \sim 10^{10}$ cm is the light cylinder for a magnetar rotating with the period P of a few seconds. As we argued above, voltage is likely near the threshold of e^\pm discharge, which gives $\Phi_e \ll 10^{11}$ V.

Therefore, we conclude that the electric current associated with observed radio emission is large, $I \gg I_{LC}$, and should flow in the closed (twisted) magnetosphere, giving a bright and relatively broad radio beam. This is consistent with the unusually broad radio pulses of magnetars, much broader than the typical pulse of ordinary pulsars with similar periods (Camilo et al. 2006; 2007). Note also that the plasma density in the twisted closed magnetosphere reaches much higher values than in the open field-line bundle, and the plasma frequency may approach the infrared band. This may explain the observed hard radio spectra.

One could consider the possibility that the radio luminosity of magnetars is generated by enhanced dissipation in the open field-line bundle and its immediate vicinity. Thompson (2008b) suggested that the diffusion of magnetic twist ψ in the closed magnetosphere initiates a strong Alfvénic turbulence near the light cylinder, with a high dissipation rate. This picture assumes that the magnetic twist tends to spread due to ohmic diffusion, as observed in normal laboratory plasma with a finite resis-

⁴ They suggested that a broad momentum distribution of relativistic particles in the open field-line bundle can evolve into a two-hump distribution as a result of resonant scattering losses, as the lower energy particles lose their energy faster than the more energetic ones. In contrast, the two-fluid flow described in Section 3 is shaped by the induced E_{\parallel} so that it sustains the electric current j ; without E_{\parallel} radiative drag would equalize the velocities of all particles at v_* .

tivity. However, later work (Beloborodov 2009; 2011a) showed that the twists in neutron-star magnetospheres evolve differently: the twist is erased “inside out” rather than spreads diffusively. The twist evolution $\partial\psi/\partial t$ is controlled by voltage induced along the magnetic field lines, Φ_e , so that $\partial\psi/\partial t \propto d\Phi_e/dF$, where F is the magnetic flux function labeling the field lines ($F = 0$ on the magnetic dipole axis). An increased voltage near the axis would imply a large negative $d\Phi_e/dF$, which implies a large negative $\partial\psi/\partial t$, i.e. rapid untwisting. Thus, the high- Φ_e twist near the open field-line bundle cannot be sustained. The ohmic effects in the closed magnetosphere can pump the twist near the open bundle only if Φ_e is *reduced* toward the magnetic dipole axis, i.e. $d\Phi_e/dF > 0$. Then the twist pumping continues until the expanding cavity $j = 0$ reaches the open bundle; a snapshot of this evolution is shown in Figure 1. The pumping of ψ leads to outbursts and spindown anomalies (Parfrey et al. 2012, 2013).

Our scenario for the low-frequency emission from magnetars may be summarized as follows. The emission is generated by the two-stream instability on the twisted closed field lines with the apex radii R_{\max} such that $R \ll R_{\max} \ll R_{LC}$. These field lines carry a large electric current $I \sim \psi c\hat{\mu}/R_{\max}^2 \gg I_{LC}$ and a modest voltage $\Phi_e \sim 10^9 - 10^{10}$ V. The high plasma density and the broad beam of radiation expected on these field lines explain the unusual radio pulsations of magnetars.

5. DYNAMICS OF OUTFLOW WITH A BROAD MOMENTUM DISTRIBUTION

5.1. Waterbag model

The plasma instability discussed in Section 4 is generated by the gradient of the distribution function df_e/dp , and the feedback of the excited plasma waves tends to make the distribution flatter. The numerical simulation in Section 4 illustrates how two interpenetrating cold fluids of e^+ and e^- with $f_e(p) = (1/2)[\delta(p-p_-) + \delta(p-p_+)]$ quickly evolve into a state with a broad and smooth $f_e(p)$. Below we design a simple modification of the two-fluid model that takes this effect into account.

The simplest model has a top-hat distribution function. In plasma physics, this approximation is often called “waterbag” model. Like the two-fluid model, the outflow is described by two parameters p_\pm (or β_\pm). However, now instead of two delta-functions we require the e^\pm distribution to be flat between p_- and p_+ ,

$$f_e(p) = \begin{cases} (p_+ - p_-)^{-1} & p_- < p < p_+ \\ 0 & p < p_- \text{ or } p > p_+ \end{cases} \quad (16)$$

This distribution includes both electrons and positrons. The plasma must be nearly neutral, $n_+ = n_-$, and the total density of particles $n = n_+ + n_-$ is given by

$$n = \frac{\dot{N}}{\beta c} = \frac{\mathcal{M}j}{e\bar{\beta}c}, \quad (17)$$

where $\dot{N} = \mathcal{M}j/e$ is the particle number flux and $\bar{\beta}$ is the average velocity,

$$\bar{\beta} = \int \beta(p) f_e(p) dp = \frac{\gamma_+ - \gamma_-}{p_+ - p_-}. \quad (18)$$

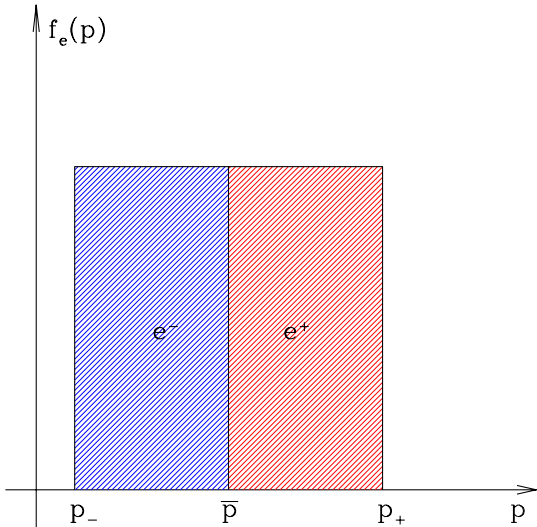


FIG. 7.— Waterbag distribution of minimum width.

Similar to the two-fluid model, p_+ and p_- are not independent, as the outflow must carry current j with a given multiplicity \mathcal{M} ; this would be impossible if, for instance, $p_+ = p_-$. The minimum possible width of the distribution function (i.e. minimum $p_+ - p_-$) is achieved if all negative charges are slower than all positive discharges, as shown in Figure 7. We will adopt this idealized momentum distribution in our numerical simulations. This is a rather crude approximation to more realistic distributions of e^+ and e^- , which overlap in momentum space (cf. Figure 6).⁵ Nevertheless, it is useful as it allows one to explore all basic features of the e^\pm outflow using a concrete relation between p_+ and p_- . This relation is determined by the outflow multiplicity \mathcal{M} . It is easy to show that the generalization of the two-fluid Equation (8) to e^\pm flows with any distribution function is given by

$$1 - \frac{\bar{\beta}_-}{\bar{\beta}_+} = \frac{2}{\mathcal{M} + 1}, \quad (19)$$

where $\bar{\beta}_+$ and $\bar{\beta}_-$ are the average velocities of the positive and negative charges, respectively. For the waterbag distribution shown in Figure 7 this condition gives

$$\frac{\bar{\beta}_-}{\bar{\beta}_+} = \frac{\gamma(\bar{p}) - \gamma_-}{\gamma_+ - \gamma(\bar{p})} = 1 - \frac{2}{\mathcal{M} + 1}, \quad \bar{p} = \frac{p_- + p_+}{2}, \quad (20)$$

where $\gamma(\bar{p}) = (1 + \bar{p}^2)^{1/2}$. Equation (20) determines the relation between p_+ and p_- (for a given \mathcal{M}); it is shown in Figure 8.

Taking into account the relation between p_+ and p_- , the outflow has essentially one degree of freedom besides

⁵ The minimum-width waterbag model may be particularly crude near the star where the outflow just begins to experience significant radiative drag. The faster positive charges will experience drag first while the slower negative charges still move freely. As p_+ decreases, the minimum-width model would require an increase in p_- . In reality, p_- may not react to the reduced p_+ until particles with $p = p_-$ also begin to experience the drag force (which is positive as $p_- < p_*$). After this point, the outflow may not be far from the “minimum-width” waterbag state.

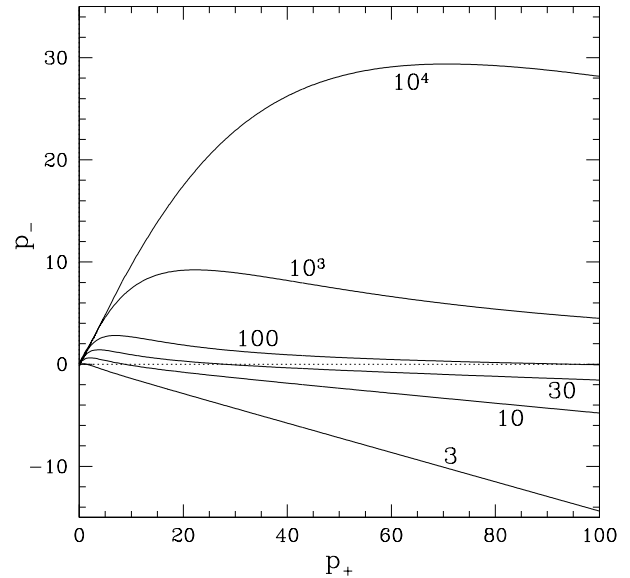


FIG. 8.— Relation between p_+ and p_- for the waterbag model shown in Figure 7. Each curve describes an outflow of a given multiplicity \mathcal{M} , which is indicated next to the curve; $p_- = 0$ is indicated by the dotted line.

the multiplicity \mathcal{M} . One can choose, e.g., p_+ as an independent variable, or any convenient combination of p_+ and p_- , $\zeta(p_+, p_-)$, that is independent from $\mathcal{M}(p_+, p_-)$. Below we will choose variable ζ and formulate the dynamic equation for ζ ; it will describe how the interaction with radiation governs the outflow dynamics along the magnetic field lines.

5.2. Momentum equation

Since the outflow is bound to move along the magnetic field lines, we will need the projection of momentum equation onto \mathbf{B} . It is convenient to write this equation in a covariant form that is valid in any curved coordinate system x^i (e.g. spherical coordinates). In a steady state, the momentum equation reads

$$\frac{B_i}{B} \nabla_k T^{ik} = \frac{dP}{dt dV}, \quad (21)$$

where $dP/dtdV$ is the rate of momentum exchange with radiation (per unit volume), ∇_k is the covariant derivative (indices i, k run from 1 to 3), and T^{ik} are the components of the plasma stress tensor,

$$T^{ik} = m_e c^2 \int u^i u^k \frac{dn}{\gamma} = n m_e c^2 \frac{B^i B^k}{B^2} \int \frac{p^2}{\gamma} f_e(p) dp. \quad (22)$$

Here $u^i = p B^i / B$ are the spatial components of the four-velocity vector of a particle with dimensionless momentum p , $dn = n f_e(p) dp$ is the number density of particles with momenta $(p, p + dp)$, and dn/γ is the corresponding density in the frame moving with $\gamma(p) = (1 + p^2)^{1/2}$. Then the left-hand side of Equation (21) takes the form,

$$\begin{aligned} \frac{B_i}{B} \nabla_k T^{ik} &= \frac{B_i}{B} \nabla_k \left(n m_e c^2 \frac{B^i B^k}{B^2} \overline{p\beta} \right) \\ &= m_e c^2 B^k \nabla_k \left(\frac{n}{B} \overline{p\beta} \right), \end{aligned} \quad (23)$$

where we used $B_i \nabla_k (B^i B^k / B) = 0$ (which follows from $\nabla_k B^k = 0$). The directional derivative $B^k \nabla_k$ equals $B d/dl$ where l is length measured along the magnetic field line. Equation (23) can be further simplified using $n\bar{\beta}/B\mathcal{M} = \text{const}$, which follows from the relation

$$n = \mathcal{M} \frac{j}{ec\bar{\beta}}, \quad (24)$$

and $j/B = \text{const}$ (cf. Equation 5). This gives

$$\frac{B_i}{B} \nabla_k T^{ik} = m_e c^2 n \frac{\bar{\beta}}{\mathcal{M}} \frac{d}{dl} \left(\frac{\mathcal{M}}{\bar{\beta}} p\bar{\beta} \right). \quad (25)$$

When $\mathcal{M} = \text{const}$ (i.e. no new pairs are created), \mathcal{M} cancels out. Finally, the substitution of Equation (25) to Equation (21) gives the momentum equation in the following form,

$$\frac{d\zeta}{dl} = \frac{\bar{\mathcal{F}}}{\bar{\beta} m_e c^2}, \quad \zeta \equiv \frac{\overline{p\bar{\beta}}}{\bar{\beta}}, \quad (26)$$

where $\bar{\mathcal{F}} = n^{-1} dP/dtdV$ is the average force exerted by radiation *per particle*. If $\bar{\mathcal{F}} = 0$ then ζ remains constant along the field lines, which implies $p_{\pm} = \text{const}$ — the momentum distribution remains unchanged along the flow.

For the waterbag model, $\bar{\beta}$ is given by Equation (18). The quantity $\overline{p\bar{\beta}}$ can also be expressed in terms of p_{\pm} , using the indefinite integral

$$\int p\bar{\beta} dp = \int p d\gamma = \frac{p\gamma}{2} - \frac{1}{4} \ln \left(\frac{1+\beta}{1-\beta} \right) + \text{const}. \quad (27)$$

This gives

$$\zeta = \frac{1}{\gamma_+ - \gamma_-} \left[\frac{1}{2} (p_+ \gamma_+ - p_- \gamma_-) - \frac{1}{4} \ln \frac{(1+\beta_+)(1-\beta_-)}{(1-\beta_+)(1+\beta_-)} \right]. \quad (28)$$

In our numerical simulations, we use ζ as the variable that describes the dynamical state of the outflow, and solve the differential Equation (26) for ζ . The values of p_{\pm} that correspond to a given ζ and \mathcal{M} are found from Equations (20) and (28).

The force $\bar{\mathcal{F}}$ experienced by an outflow with a given ζ is determined by the local radiation field, which is described by the intensities in the two polarization modes $I_{\perp}(\omega, \mathbf{n})$ and $I_{\parallel}(\omega, \mathbf{n})$ (Appendix A). In general, the force acting on a plasma with a distribution function $f_e(p)$ is given by Equation (A20). Force $\bar{\mathcal{F}}$ is easily calculated in the simple case of an optically thin magnetosphere exposed to the central blackbody radiation (Appendix B). Then the right-hand side of Equation (26) is a known function of ζ and it is straightforward to numerically solve this equation; the results are similar to the two-fluid model described in Section 4. The optically thin approximation is, however, invalid for active magnetars. The radiation is not central; instead I_{\perp} and I_{\parallel} must be calculated self-consistently, together with the outflow dynamics. This requires radiative transfer simulations.

Note that we assume here that $p_{\pm} > 0$, so that all particles move away from the star until they reach the equatorial plane and disappear (annihilate) there. This approximation is reasonable for the flow along the extended field lines with apex radii $R_{\text{max}} \gtrsim 10R$. Near the apexes, i.e. near the equatorial plane $\theta = \pi/2$, the

radiative drag enforces $p_{\pm} \approx p_{\star} \ll 1$, creating a dense layer of slow particles where they annihilate (Fig. 2). A more general model of the flow could allow the particles to cross the equatorial plane and enter the opposite hemisphere. By symmetry, this would be equivalent to the reflection boundary condition, i.e. the mirror image of the outflow approaching the equatorial plane would emerge from the equatorial plane. Then the distribution function $f_e(p)$ must extend to negative p . This modification would be required for the plasma flow on field lines with small R_{max} , where radiative drag is less efficient and the plasma can cross the equatorial plane with a large p . In this paper, we focus on the field lines with $R_{\text{max}} \gtrsim 10$, where this does not happen. The field lines with small R_{max} are assumed to form a cavity with $j = 0$ and a negligible plasma density (Figure 1).

6. SELF-CONSISTENT RADIATIVE TRANSFER

The problem of radiative transfer in a relativistically moving e^{\pm} plasma whose velocity is controlled by the radiation field is not unique to magnetars. A similar situation may occur in accretion disk outflows (Beloborodov 1998) and gamma-ray bursts (Beloborodov 2011b). The strong radiative drag (measured by the coefficient $\mathcal{D} \gg 1$, Equation [4]) was previously shown to simplify the problem, as it forces the plasma to keep the saturation momentum p_{\star} such that the net radiation flux vanishes in the plasma rest frame. This ‘‘equilibrium’’ transfer has one additional integral compared with the classical Chandrasekhar-Sobolev transfer problem for a medium at rest. The transfer in magnetar magnetospheres has, however, two special features that complicate the problem. First, the electric current and plasma instabilities imply additional (electric) forces that broaden the momentum distribution around p_{\star} , as discussed in Sections 4 and 5. Therefore, the equilibrium condition $p = p_{\star}$ is not satisfied even where $\mathcal{D} \gg 1$. Second, opacity is dominated by *resonant* scattering, whose rate is sensitive to the particle momentum. Below we develop a method to solve the self-consistent transfer for magnetars.

6.1. Monte-Carlo technique and the ‘‘virtual beam’’ method

Radiative transfer in a magnetosphere filled with plasma with given parameters can be calculated using the standard Monte-Carlo technique (e.g. Fernández & Thompson 2007; Nobili, Turolla & Zane 2008). Blackbody photons are injected into the magnetosphere at the neutron-star surface and their trajectories are followed until they escape the magnetosphere. We implement this method using the scattering opacity given in Appendix A and keeping track of the photon polarization, which can switch in the scattering events.

Calculation of transfer in an outflow with self-consistent dynamics is a more ambitious goal, as the plasma parameters are not known in advance. A natural approach is iterative. One can start with a trial outflow, calculate radiative transfer to find the radiation intensity that would correspond to this outflow, and then re-calculate the outflow dynamics in the obtained radiation field. These iterations can be repeated until they converge. The problem is simplified for the waterbag

plasma model (Section 5) as the outflow is described by one dynamic variable ζ . As the first trial initiating the iterations one can take the outflow solution $\zeta(r, \theta)$ for the optically thin magnetosphere exposed to the central blackbody radiation.

One then encounters the following difficulty. For the calculation of next iteration of outflow dynamics, one needs to know $I_{\perp}(\mathbf{r}, \omega, \mathbf{n})$ and $I_{\parallel}(\mathbf{r}, \omega, \mathbf{n})$ everywhere in the magnetosphere. In axisymmetric magnetospheres, the radiation intensity is a function of five variables: two for location (radius r and polar angle θ), one for spectrum (ω), and two for angular distribution (unit vector \mathbf{n} is described by two angles). To determine intensities I_{\perp} and I_{\parallel} with sufficient accuracy, one has to introduce a five-dimensional grid and accumulate large photon statistics for each grid cell during the Monte-Carlo simulation of radiative transfer. A grid of size N for each of the five variables has N^5 cells. Accumulation of photon statistics in each cell requires the calculation of a huge number of Monte-Carlo realizations of the photon trajectory in the magnetosphere. This is expensive and gives poor accuracy.

There is, however, a more efficient method that does not require the knowledge of intensities $I_{\perp, \parallel}(\mathbf{r}, \omega, \mathbf{n})$. They are not, in fact, needed for the calculation of outflow dynamics. What enters the momentum Equation (26) is the average force $\bar{\mathcal{F}}(r, \theta)$, which may be tabulated in the two-dimensional space of r, θ . This force can be calculated directly during the Monte-Carlo simulation of radiative transfer if we find a way to evaluate the contribution of each simulated photon to $\bar{\mathcal{F}}(r, \theta)$ as it propagates through the magnetosphere.

This can be achieved if we imagine that the photon is replaced by a beam of radiation. As we follow the photon along its trajectory, we can calculate the force that would be applied by the imaginary beam to any given outflow that can be imagined in the magnetosphere. In the waterbag model, the outflow is described by one dynamical parameter ζ , and so the force applied by the beam can be tabulated on a grid of ζ .

Once we know how to calculate the force created by each photon trajectory in our Monte-Carlo simulation, we should be able to average it over all simulated photons and thus accurately evaluate $\bar{\mathcal{F}}(r, \theta, \zeta)$. This gives the force that *would be* applied by our radiation field to an outflow with any given ζ at any point r, θ . At the next iteration step $\bar{\mathcal{F}}(r, \theta, \zeta)$ is used to obtain the new outflow solution $\zeta(r, \theta)$ by integrating the momentum equation $d\zeta/dl = W(l, \zeta)$, where $W = \bar{\mathcal{F}}/\beta m_e c^2$ (Equation 26). Then the Monte-Carlo simulation can be repeated to calculate radiative transfer in the new outflow and find $\bar{\mathcal{F}}(r, \theta, \zeta)$ for the new radiation field. These steps can be repeated until the outflow solution $\zeta(r, \theta)$ converges, i.e. remains practically unchanged by new iterations.

The concrete implementation of this strategy is as follows. Let L_{th} be the thermal luminosity of the star and $\dot{N} = L_{\text{th}}/2.7kT$ be the number of photons emitted by the star per unit time. In our Monte-Carlo simulation we follow $K_{\text{MC}} \sim 10^7$ random photon trajectories. This can be thought of as dividing \dot{N} into K_{MC} random monochromatic beams. Each beam has a random start at the star surface (the photon energy is drawn from the Planck

distribution) and follows one random realization of the photon trajectory, which can involve multiple scattering events in the magnetosphere. The photon number flux in each monochromatic beam is $\dot{N}_b = \dot{N}/K_{\text{MC}}$, and the energy flux in the beam is

$$\dot{E}_b = \dot{N}_b \hbar \omega. \quad (29)$$

Note that $\dot{N}_b = \text{const}$ along the beam (i.e. along the photon trajectory in the Monte-Carlo simulation) while the photon energy $\hbar \omega$ changes after each scattering in the magnetosphere. The collection of K_{MC} beams represent the state of the radiation field around the star.

As we follow each realization of the photon trajectory, in parallel we calculate the force applied by the virtual beam to the plasma. We can imagine that the beam has a small cross section A (it will cancel in the final result) and flux density $F = \dot{E}_b/A$. Equation (A19) gives a general expression for the force exerted by radiation on a plasma with a given distribution function $f_e(p)$. For a monochromatic beam of frequency ω propagating at angle ϑ with respect to the magnetic field, this expression gives the following momentum deposition rate,

$$\frac{dP}{dt dV} = 2\pi^2 r_e n F \xi \frac{\omega_B}{\omega^2} [\gamma_1 f_e(p_1) - \gamma_2 f_e(p_2)], \quad \omega \sin \vartheta \leq \omega_B, \quad (30)$$

($dP/dt dV = 0$ if $\omega \sin \vartheta > \omega_B$), where

$$p_{1,2}(\omega, \vartheta) = \frac{\omega_B}{\omega \sin^2 \vartheta} \left(\cos \vartheta \mp \sqrt{1 - \frac{\omega^2}{\omega_B^2} \sin^2 \vartheta} \right), \quad (31)$$

and the factor ξ depends on the beam polarization,

$$\xi = \begin{cases} 1, & \perp \\ 1 - \frac{\omega^2}{\omega_B^2} \sin^2 \vartheta, & \parallel \end{cases} \quad (32)$$

The rate of momentum deposition by the beam (i.e. the exerted force) per unit length along its trajectory is given by

$$\frac{dP}{dt ds} = \frac{dP}{dt dV} A. \quad (33)$$

We need to tabulate the force on a spatial grid, which is used to calculate the outflow dynamics at the next iteration. Therefore, we need to evaluate the net force applied to a given spatial cell. The number of particles in the cell is nV_c where V_c is the cell volume, and the force exerted by the beam *per particle* in the cell is given by

$$\frac{d\bar{\mathcal{F}}_b}{ds} = \frac{1}{nV_c} \frac{dP}{dt ds} = 2\pi^2 \frac{r_e}{V_c} \frac{\omega_B \dot{E}_b}{\omega^2} \xi [\gamma_1 f_e(p_1) - \gamma_2 f_e(p_2)]. \quad (34)$$

In the transfer calculation, we track the photon trajectory using small steps δs , much smaller than the cells of the spatial grid. To obtain the force $\bar{\mathcal{F}}_b(r, \theta, \zeta)$ applied by the beam in a given cell we integrate Equation (34) along the photon path where it crosses the cell. Note that a finer spatial grid implies a larger $d\bar{\mathcal{F}}_b/ds \propto V_c^{-1}$; however, it also implies that the cell is less frequently visited by photons in our Monte-Carlo simulation, and the photons spend a shorter time in the cell; therefore, the final result does not depend on the grid.

In an axisymmetric magnetosphere, the spatial cells (i, j) are tori of volume $V_{i,j} = 2\pi r_i^2 \sin\theta_j \Delta r \Delta\theta$. The net force applied per particle in a given cell (i, j) is obtained by summing up the contributions $\bar{\mathcal{F}}_b(r_i, \theta_j, \zeta)$ from all simulated beams,

$$\bar{\mathcal{F}}(r_i, \theta_j, \zeta) = \frac{\dot{N}}{K_{\text{MC}}} \sum_{k=1}^{K_{\text{MC}}} \frac{2\pi r_e \hbar}{V_{i,j}} \times \int_{\text{cell}(i,j)} \frac{\omega_B}{\omega} \xi [\gamma_1 f_e(p_1) - \gamma_2 f_e(p_2)] ds. \quad (35)$$

Note that the beam may cross a given cell multiple times in an opaque magnetosphere, and all crossings contribute to the path integral in Equation (35). The e^\pm distribution function $f_e(p)$ is determined by the parameter ζ (assuming a given pair multiplicity \mathcal{M} , see Section 5).

As a test, one can apply Equation (35) to the simplest case of a transparent outflow exposed to the central thermal radiation. Then the expected $\bar{\mathcal{F}}$ can be directly calculated using Equation (B17) in Appendix B. We analytically verified that in this case Equation (35) is reduced to Equation (B17). We also tested our numerical code; it reproduced the analytical result.

6.2. Results

The obtained self-consistent solution for the outflow dynamics is shown in Figure 9. We show p_+ rather than our dynamical parameter ζ , because p_+ is closely related to the radiation emitted by the outflow. We find that only particles with the highest momenta $p \approx p_+$ resonantly scatter thermal photons in the relativistic zone $p_+ > 1$; the remaining, dominant part of the momentum distribution does not participate in scattering. The Lorentz factor of the scattering particles is

$$\gamma_{\text{sc}} \approx (1 + p_+^2)^{1/2}. \quad (36)$$

The solution $p_+(r, \theta)$ shown in Figure 9 was calculated assuming that the star has radius $R = 10$ km, a uniform surface temperature $kT = 0.3$ keV, and a moderately twisted dipole magnetic field with $B_{\text{pole}} = 10^{15}$ G and $\psi = 0.3$; the multiplicity of the e^\pm flow was fixed at $\mathcal{M} = 200$. The flow is injected at $r = 2R$ with $p_+(2R) = 100$. The choice of the boundary condition is not important as we are interested in the flow behavior outside $\sim 5R$, where the scattered photons avoid conversion to e^\pm pairs and can escape, i.e. where the observed hard X-rays are produced (Beloborodov 2013). For any reasonable boundary value $p_+(2R)$, the flow relaxes to the same solution $p_+(r, \theta)$ outside a few stellar radii. Remarkably, our simulations gave practically the same solution for a broad range of parameters ψ , \mathcal{M} , T that is relevant for magnetars. This demonstrates a robust self-regulation mechanism; this important feature is explained below (see also the accompanying paper).

There are two distinct zones in the outflow:

I. Non-relativistic zone $p_+ \ll 1$, which is near the equatorial plane (red zone in Figure 9). This zone has a huge optical depth and scatters essentially all thermal photons that impinge on it from the star ($\sim 10\%$ of the thermal luminosity L_{th}). We will call this zone the “equatorial reflector.”

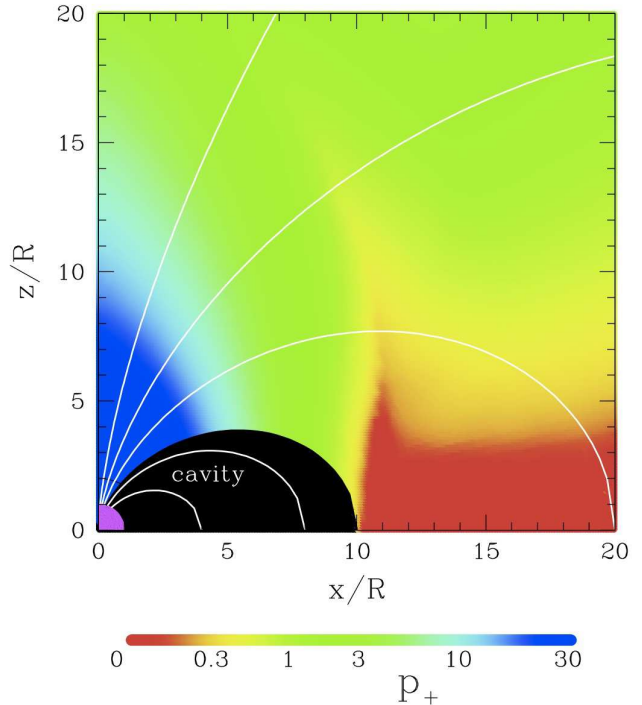


FIG. 9.— Self-consistent outflow solution. Color shows the parameter p_+ of the waterbag distribution function. Observed hard X-rays (discussed in the accompanying paper Beloborodov (2013)), are produced by particles with $p \approx p_+$. The simulation assumed that the active j-bundle occupies the field lines with apex radii $R_{\text{max}} > 10R$ (Section 1).

II. Relativistic zone $p_+ > 1$ (blue to green in Figure 9). This zone is transparent for essentially all thermal photons flowing from the star, except for rare photons in the far Wien tail of the Planck spectrum, which may be neglected. Basically, the outflow in this zone does not “see” the thermal radiation flowing from the star. It mainly interacts with (and is decelerated by) the quasi-thermal photons that flow from the equatorial equator.

It is easy to see why the outflow in the relativistic zone $\gamma_+ \gg 1$ is regulated so that it interacts with a tiny fraction of the thermal photons around the magnetar. Scattering on average boosts the energy of a thermal photon $\hbar\omega$ by a factor comparable to γ^2 , and hence the energy lost by the outflow per scattering is $\sim \gamma^2 \hbar\omega$. If we imagine that each thermal photon is scattered once with an average blueshift of γ^2 , the generated hard X-ray luminosity $\gamma^2 L_{\text{th}}$ would exceed the kinetic power of the outflow L , which is impossible. The scattering rate must be kept low, just sufficient for the self-consistent gradual deceleration of the outflow. The outflow “vision” of targets for scattering is controlled by the resonance condition $\gamma(1 - \beta \cos\vartheta)\omega = \omega_B$, where ϑ is the angle between the photon direction and the particle velocity $\vec{\beta}$. The scattering rate is greatly reduced if γ is so low that the resonance condition is satisfied only for rare photons in the Wien tail of the thermal spectrum. The situation may be compared with the regulation of the nuclear burning rate in the sun. The self-consistent temperature is sufficiently low so that fusion reactions occur only in the far tail of the Maxwell distribution; as a result only rare particles participate in burning, and these particles

are concentrated in a narrow interval of (large) momenta, a phenomenon known as the Gamow peak. Similarly, our self-consistent outflow moves sufficiently slow so that resonant scattering is only enabled between rare particles with the highest $p \approx p_+$ and rare thermal photons with the highest energies in the particle rest frame. These lucky photons have the largest ϑ (gained after reflection from the equatorial reflector) and large $\hbar\omega \gg 2.7kT$. The inward direction ($\cos\vartheta < 0$) of the reflected photons gives them particularly large blueshift in the outflow rest frame and hence reduces the energy requirement in the lab frame. This makes the reflected photons the dominant targets for scattering even though their density is much smaller than the density of photons flowing directly from the star. The reflected photons have a diluted quasi-thermal spectrum of temperature T .

In essence, we observe in our simulations that the outflow moves fast enough to resonantly interact with reflected photons of energy $\hbar\omega \sim (7 - 10)kT$ (the low-density exponential tail of the thermal spectrum), and slow enough to not interact with the main peak of the reflected thermal spectrum $\hbar\omega \sim 3kT$. This condition, together with the resonance condition $\gamma(1 - \beta \cos\vartheta)\omega = \omega_B$ and $\cos\vartheta \sim -0.5$, determines that the scattering plasma moves with Lorentz factor

$$\gamma_{\text{sc}} \approx \frac{m_e c^2}{10kT} \frac{B}{B_Q}, \quad (37)$$

as long as $\gamma_{\text{sc}} \gg 1$. In this regime, the number of target photons visible to an outflowing particle has a strong exponential sensitivity to the particle momentum p . Essentially all scattering must be done by particles with the highest momenta in the distribution function, i.e. with $p \approx p_+$ for the waterbag distribution, as indeed observed in our numerical simulation. Therefore, γ_{sc} is associated with p_+ . Equation (37) serves as a simple and reasonably accurate approximation to the exact numerical results shown in Figure 9. Its applicability is not limited to the specific simulation with its B_{pole} , T , ψ , \mathcal{M} — the approximation works well for other magnetar parameters, because of the robust self-regulation effect described above. This fact is further discussed and illustrated in Figure 2 in Beloborodov (2013).

Besides Equation (37), the transfer problem is characterized by the position of the equatorial reflector. It is described by a simple formula, which can be used to scale the results shown in Figure 9 to models with other parameters. The formula is based on the following fact (see Appendix B): if a given active magnetic loop extends to the region where $\hbar\omega_B < 20kT$, the central thermal radiation exerts a sufficiently strong drag on the outflow to bring it to rest at the top of the loop. The region $\hbar\omega_B < 20kT$ corresponds to $r > R_1$ where

$$R_1 \approx 80 \left(\frac{\hat{\mu}}{10^{33} \text{ G cm}^3} \right)^{1/3} \left(\frac{kT}{1 \text{ keV}} \right)^{-1/3} \text{ km}. \quad (38)$$

Here $\hat{\mu} = R^3 B_{\text{pole}}/2$ is the magnetic dipole moment of the star. Equation (38) describes the position of the inner edge of the non-relativistic (red) zone; e.g. the model in Figure 9 has $R_1 \approx 10R$.

It is instructive to compare the result of the full transfer calculation in Figure 9 with the simplest, optically thin two-fluid model in Figure 3. The relativistic zone

$p_+ > 1$ remains practically transparent to thermal radiation. The key difference is the presence of the opaque equatorial reflector. The reflector weakly affects the spectrum of thermal photons supplied by the star, however it significantly changes their angular distribution in the magnetosphere. As a result, the radiation exerts a stronger drag on the outflow and p_+ decreases faster along the magnetic field lines. In Figure 3, $\gamma_+ \approx p_+ \gg 1$ remains huge near the magnetic axis — the central radiation is unable to decelerate the plasma because the photons flow from behind and have small angles ϑ with respect to the plasma velocity. In Figure 9, the equatorial reflector supplies photons with large ϑ , which efficiently decelerate the outflow, according to Equation (37).

The upscattered photons of energy $E \sim \gamma^2 E_t$ are beamed along the relativistic outflow. Therefore, they become unable to decelerate the plasma, even though they can scatter multiple times before escaping. The outflow significantly loses energy when it scatters a photon propagating at a large angle ϑ with respect to the outflow velocity; only in this case the scattering boosts the photon energy by the factor of $\sim \gamma_{\text{sc}}^2 \gg 1$. After the scattering, the photon angle is reduced to $\vartheta \sim \gamma_{\text{sc}}^{-1}$, and its subsequent scatterings have a small effect on the outflow dynamics. The beamed radiation initially moves together with the plasma and then escapes. Our transfer simulations include all scattering events, however practically the same $p_+(r, \theta)$ would be obtained if only single scattering were allowed in the relativistic zone $p_+ \gg 1$.

7. CONCLUSIONS

This paper examined the behavior of the relativistic plasma created by e^\pm discharge around magnetars. Plasma circulation in the magnetosphere is schematically shown in Figure 2. We focused on large magnetic loops, which must be heavily loaded with e^\pm pairs. The plasma momentum is controlled by the radiation field around the star, which interacts with e^+ and e^- via resonant scattering. We developed a method to calculate radiative transfer in the self-consistently moving plasma and obtained the solution for the e^\pm flow (Figure 9). The solution is a strong attractor — the behavior of the plasma outside a few stellar radii does not depend on how the plasma is injected near the star and its initial Lorentz factor γ_0 , as long as $\gamma_0 \gg 30$ ($\gamma_0 \gtrsim 10^3$ is expected, which corresponds to the discharge voltage $\Phi_e \sim 10^9$ V). The e^\pm flow shows the following features:

(1) The relativistic flow scatters radiation with a well defined Lorentz factor γ_{sc} given in Equation (37); γ_{sc} decreases proportionally to B along the magnetic field lines.

(2) The relativistic flow remains transparent to thermal photons emitted by the star until it decelerates to non-relativistic momenta $p < 1$. The non-relativistic zone is opaque to the star radiation and forms the “equatorial reflector” (red zone in Figure 9).

(3) The energy lost by the decelerating flow is converted to hard X-rays. The resulting emission is calculated and compared with observations in the accompanying paper (Beloborodov 2013).

(4) The plasma is nearly neutral, $n_+ \approx n_-$, and carries the electric current $\mathbf{j} = (c/4\pi)\nabla \times \mathbf{B}$ by adjusting the particle velocities. In large magnetic loops (extending

to the region of $B \lesssim 10^{13}$ G) the plasma has a high e^\pm multiplicity $\mathcal{M} \sim 10^2$, and both electrons and positrons outflow from the neutron star, with a small separation in the velocity space. This separation is sustained by a modest electric field induced along the magnetic field lines.

(5) The enforced electric current and radiative drag together create a configuration that is prone to two-stream instability, which is expected to generate low-frequency

radiation. The mechanism of initiating the two-stream instability is unique to magnetars, explaining their special radio emission and possibly optical/UV emission.

This work was supported by NASA grants NNX-10-AI72G and NNX-13-AI34G. I thank R. Hascoët for comments on the manuscript.

APPENDIX

A. RESONANT SCATTERING

Resonant scattering plays a significant role in ordinary pulsars (e.g. Kardashev, Mitrofanov, & Novikov 1984; Daugherty & Harding 1989; Sturmer 1995; Lyubarsky & Petrova 2000). It is also the dominant radiative process in magnetar magnetospheres, which governs the radiative transfer calculated in this paper. Below we summarize basics of resonant scattering, write down the cross section, the optical depth of the e^\pm flow, and the radiative drag force that are used in our numerical simulations.

Photons scattered in the region $B > 10^{13}$ G are immediately absorbed (Beloborodov 2013). Interesting radiative transfer occurs outside this region, where $B \ll B_Q$. In particular, the observed hard X-rays of energy up to several MeV are radiated where $B \ll B_Q$. Electron recoil is small for resonant scattering in such relatively weak fields, and the scattering cross section is particularly simple.

A.1. Scattering cross section

In classical language, the electro-magnetic wave (photon) with frequency $\omega_B = eB/m_e c$ resonates with the Larmor rotation of electron. Then the wave strongly accelerates the charged particle and generates scattered radiation. The corresponding cross section is largest for waves with the right-hand circular polarization $\mathbf{e} = \mathbf{e}_-$ that matches the electron Larmor rotation. Here $\mathbf{e}_- = 2^{-1/2}(\mathbf{e}_x - i\mathbf{e}_y)$ and $\{\mathbf{e}_x, \mathbf{e}_y, \mathbf{e}_z\}$ is a Cartesian basis with the z -axis anti-parallel to \mathbf{B} . For a wave with an arbitrary polarization vector \mathbf{e} , only the projection of \mathbf{e} on \mathbf{e}_- is responsible for the resonance, and the cross section is reduced by the factor $|\mathbf{e}^* \cdot \mathbf{e}_-|^2$, where \mathbf{e}^* is the complex conjugate of \mathbf{e} . In quantum language, the resonance occurs because the photon energy matches the energy $\hbar\omega_B$ needed for the electron transition from the ground Landau state to the first excited state. The resonance has a finite width. It equals the natural width of the cyclotron line Γ , which corresponds to the lifetime of the excited electron to spontaneous transition back to the ground Landau state.

For an electron at rest, the differential cross section for photon scattering into solid angle $d\Omega'$ is given by (Canuto et al. 1971; Ventura 1979),

$$\frac{d\sigma}{d\Omega'} = r_e^2 \frac{\omega^2}{(\omega - \omega_B)^2 + (\Gamma/2)^2} |\mathbf{e}^* \cdot \mathbf{e}_-|^2 |\mathbf{e}'^* \cdot \mathbf{e}_-|^2, \quad (\text{A1})$$

where $r_e = e^2/m_e c^2$, ω is the photon frequency, \mathbf{e} and \mathbf{e}' are the polarization vectors of the photon before and after scattering. Equation (A1) retains only the resonance peak of the cross section and neglects the non-resonant part. Positron cross section is described by the same equation except that \mathbf{e}_- is replaced by $\mathbf{e}_+ = 2^{-1/2}(\mathbf{e}_x + i\mathbf{e}_y)$ (positrons gyrate in the opposite sense). The cross section can also be derived in the framework of quantum electrodynamics (Herold 1979; Daugherty & Harding 1986). For $\hbar\omega_B \ll m_e c^2$ (which corresponds to $B \ll B_Q$) the result is reduced to Equation (A1).

The resonance line is very narrow, $\Gamma/\omega_B = (4/3)\alpha(B/B_Q) \ll 1$, where $\alpha = e^2/\hbar c = 1/137$ (Daugherty & Ventura 1978; Herold et al. 1982), and the resonance factor $[(\omega - \omega_B)^2 + (\Gamma/2)^2]^{-1}$ is well approximated by the delta-function $2\pi\Gamma^{-1}\delta(\omega - \omega_B)$. Then the cross section may be written as

$$\frac{d\sigma}{d\mu'} = 2\pi \frac{d\sigma}{d\Omega'} = 3\pi^2 r_e c \delta(\omega - \omega_B) |\mathbf{e}^* \cdot \mathbf{e}_\pm|^2 |\mathbf{e}'^* \cdot \mathbf{e}_\pm|^2, \quad (\text{A2})$$

where $+/-$ correspond to scattering by positron/electron, $\mu' = \cos\vartheta'$, and ϑ' is the angle of the scattered photon with respect to the magnetic field \mathbf{B} . The distribution of scattered photons is axially symmetric about \mathbf{B} ; this fact has been used in Equation (A2).

Two polarization states (eigen modes) exist for the photon. They are controlled by the dielectric tensor of the magnetosphere. In the considered region $r < 100R$, the dielectric tensor for photons of interest (X-rays) is dominated by the magnetic vacuum polarization effect (e.g. Beresteskii et al. 1982); the plasma contribution to the dielectric tensor is much smaller and may be neglected. Magnetic vacuum defines two linearly polarized eigen modes for electromagnetic waves: \mathbf{e}_\perp which is perpendicular to the (\mathbf{k}, \mathbf{B}) plane, and \mathbf{e}_\parallel which is parallel to the (\mathbf{k}, \mathbf{B}) plane (here \mathbf{k} is the photon wave vector and \mathbf{e} shows the direction of the electric field in the wave). The \perp and \parallel modes are also called E-mode and O-mode, respectively. Their refraction indices are

$$N_\perp = 1 + \frac{2\alpha}{45\pi} \left(\frac{B}{B_Q}\right)^2 \sin^2\vartheta, \quad N_\parallel = 1 + \frac{7\alpha}{90\pi} \left(\frac{B}{B_Q}\right)^2 \sin^2\vartheta, \quad (\text{A3})$$

where ϑ is the photon angle with respect to \mathbf{B} . The two modes have slightly different propagation speeds c/N and therefore they adiabatically track, i.e. the photon propagating through the curved magnetic field preserves its polarization state. The adiabaticity condition reads $kl_B(N_{\parallel} - N_{\perp}) \gg 1$ where $l_B \sim r$ is the characteristic scale of the spatial variation of \mathbf{B} (see e.g. Fernández & Davis 2011 for a detailed discussion). This condition is satisfied for X-rays in the considered region of the magnetosphere where scattering occurs. Thus, in our transfer problem, the photon can switch its polarization state only in a scattering event.

As the photon can be in either polarization state, calculation of radiative transfer involves four scattering processes $\perp \rightarrow \perp$, $\perp \rightarrow \parallel$, $\parallel \rightarrow \perp$, and $\parallel \rightarrow \parallel$. The corresponding cross sections are given by Equation (A2) with $|\mathbf{e}_{\perp}^* \cdot \mathbf{e}_{\pm}|^2 = |\mathbf{e}'_{\perp} \cdot \mathbf{e}_{\pm}|^2 = 1/2$, $|\mathbf{e}_{\parallel}^* \cdot \mathbf{e}_{\pm}|^2 = \mu^2/2$, and $|\mathbf{e}'_{\parallel} \cdot \mathbf{e}_{\pm}|^2 = \mu'^2/2$. Note that the cross sections of electron and positron are equal, as $|\mathbf{e}^* \cdot \mathbf{e}_{-}|^2 = |\mathbf{e}^* \cdot \mathbf{e}_{+}|^2$ for any linear polarization \mathbf{e} .

Equation (A2) describes the cross section of electron (or positron) at rest. In our transfer problem, the particles are moving along \mathbf{B} and the above equations should be used in the rest frame of the particle. Note that the polarization states and ω_B are invariant under Lorentz boosts along \mathbf{B} . Consider a photon with energy $\hbar\omega$ and propagation angle ϑ with respect to \mathbf{B} , in the \perp or \parallel polarization state. We are interested in its scattering by an electron (or positron) that moves with velocity βc along the magnetic field line. The total cross section in the lab frame may be obtained by integrating the differential cross section in the electron rest frame and then multiplying the result by $1 - \beta \cos \vartheta$,

$$\sigma_{\text{tot}} = 2\pi^2 r_e c \xi \delta(\tilde{\omega} - \omega_B) (1 - \beta\mu), \quad (\text{A4})$$

where

$$\tilde{\omega} = \gamma(1 - \beta\mu)\omega, \quad (\text{A5})$$

is the photon frequency in the electron rest frame and $\mu = \cos \vartheta$. The factor ξ depends on the photon polarization and is given by

$$\xi \equiv \left\{ \begin{array}{l} 1, \quad \perp \\ \tilde{\mu}^2, \quad \parallel \end{array} \right\}, \quad \tilde{\mu} = \frac{\mu - \beta}{1 - \beta\mu}, \quad (\text{A6})$$

where $\tilde{\mu} = \cos \tilde{\vartheta}$ and $\tilde{\vartheta}$ is the photon angle with respect to \mathbf{B} in the electron rest frame. The cross section σ_{tot} is summed over the final polarization states.

The outcome of the scattering may be either \perp or \parallel photon propagating at angle $\tilde{\vartheta}'$ in the electron frame. The probability distribution for $\tilde{\mu}' = \cos \tilde{\vartheta}'$ is given by

$$P(\tilde{\mu}') = \frac{1}{\sigma_{\text{tot}}} \frac{d\sigma}{d\tilde{\mu}'} = \frac{3}{8} \xi'. \quad (\text{A7})$$

where $\xi' = 1$ or $\tilde{\mu}'^2$, depending on the final polarization state. The integral $\int P(\tilde{\mu}') d\tilde{\mu}'$ equals 3/4 for the \perp state and 1/4 for the \parallel state. Thus, 3/4 of scattering events produce \perp photons with uniform distribution $P(\tilde{\mu}') = \text{const}$ and the remaining 1/4 of scattering events produce \parallel photons with $P(\tilde{\mu}') \propto \tilde{\mu}'^2$. The distribution of the final photons over angle and polarization does not depend on the initial state of the photon before scattering.

The standard description of resonant scattering summarized above assumes the transition between the ground and first excited Landau levels, which has the largest cross section. Transitions to higher levels are neglected in our transfer calculations.

A.2. Opacity

Optical depth of a relativistic plasma to resonant scattering was discussed previously in detail (e.g. Fernández & Thompson 2007 and refs. therein). Here we write down relevant equations and introduce notation that is used below in the discussion of radiative drag. Consider a photon of energy $\hbar\omega$ that propagates through e^{\pm} plasma with density $n = n_+ + n_-$. The plasma particles move along \mathbf{B} with momentum distribution $f_e(p)$ that is normalized to unity

$$\int f_e(p) dp = 1. \quad (\text{A8})$$

The optical depth $d\tau$ seen by the photon as it propagates distance ds is given by

$$\frac{d\tau}{ds} = n \int \sigma_{\text{tot}} f_e(p) dp. \quad (\text{A9})$$

Assuming that the magnetosphere has a small optical depth to non-resonant scattering (Appendix C), we include only resonant scattering and use Equation (A4) for σ_{tot} . Integration over p may be carried out using the identity,

$$\delta(\tilde{\omega} - \omega_B) = \sum_k \frac{\delta(p - p_k)}{|d\tilde{\omega}/dp|}, \quad (\text{A10})$$

where

$$\frac{d\tilde{\omega}}{dp} = \frac{d}{dp} (\gamma - p\mu) \omega = (\beta - \mu)\omega, \quad (\text{A11})$$

and p_k are all possible solutions of equation $\tilde{\omega}(p) = \omega_B$. The delta-functions $\delta(p - p_k)$ express the fact that the photon is scattered by electrons or positrons with momenta p_k for which the resonance condition is met. The relation $\tilde{\omega} \sin \tilde{\vartheta} = \omega \sin \vartheta$ together with the resonance condition $\tilde{\omega} = \omega_B$ determines $\sin \tilde{\vartheta} = (\omega/\omega_B) \sin \vartheta$ and leaves two possibilities for $\tilde{\mu} = \cos \tilde{\vartheta}$,

$$\tilde{\mu} = \pm \left(1 - \frac{\omega^2}{\omega_B^2} \sin^2 \vartheta \right)^{1/2}. \quad (\text{A12})$$

Angle $\tilde{\vartheta}$ exists (i.e. the resonance is in principle possible) for photons that satisfy the condition $\omega \sin \vartheta \leq \omega_B$. Then Equation (A12) defines two electron velocities $\beta_{1,2}$, which may be found from the Doppler transformation of the photon angle, $\tilde{\mu} = (\mu - \beta)/(1 - \beta\mu)$. It yields,

$$\beta = \frac{\mu - \tilde{\mu}}{1 - \mu\tilde{\mu}}, \quad \beta_{1,2} = \frac{\mu \mp |\tilde{\mu}|}{1 \mp \mu|\tilde{\mu}|}. \quad (\text{A13})$$

The corresponding Lorentz factors $\gamma = (1 - \beta^2)^{-1/2}$ and dimensionless momenta $p = \gamma\beta$ are

$$\gamma_{1,2} = \frac{1 \mp \mu|\tilde{\mu}|}{\sin \vartheta \sin \tilde{\vartheta}}, \quad p_{1,2} = \frac{\mu \mp |\tilde{\mu}|}{\sin \vartheta \sin \tilde{\vartheta}}. \quad (\text{A14})$$

Substitution of Equations (A4) and (A10) to Equation (A9) and integration over p gives

$$\frac{d\tau}{ds} = 2\pi^2 r_e \frac{c}{\omega} \frac{\xi}{|\tilde{\mu}|} n [f_e(p_1) + f_e(p_2)]. \quad (\text{A15})$$

Here $\xi = 1$ for \perp photons and $\xi = \tilde{\mu}^2$ for \parallel photons (Equation A6).

A.3. Radiative drag force

Consider now a radiation field with intensity $I(\omega, \mathbf{k})$ in a given polarization state, \perp or \parallel . As a result of scattering, radiation exerts a force on the e^\pm plasma. We are interested in the component of this force along the magnetic field. The force applied to unit volume of the plasma is given by

$$\frac{dP}{dt dV} = \int d\Omega \int d\omega \int dp \frac{I(\omega, \mathbf{k})}{\hbar\omega} n f_e(p) \sigma_{\text{tot}} \Delta P. \quad (\text{A16})$$

Here $\int d\Omega$ is the solid-angle integration over photon directions $\mathbf{n} = \mathbf{k}/k$, and ΔP is the average momentum (per scattering) passed to an electron or positron with Lorentz factor γ by a photon (ω, \mathbf{k}) . In the electron rest frame, $\Delta \tilde{P}$ equals the photon momentum along \mathbf{B} , as its average momentum after scattering vanishes (resonant scattering is symmetric in the electron frame when $\hbar\omega_B \ll m_e c^2$). Thus, $\Delta \tilde{P} = \tilde{\mu} \hbar\omega/c$ and the Lorentz transformation of the four-momentum vector to the lab frame gives

$$\Delta P = \gamma \tilde{\mu} \frac{\hbar\omega_B}{c}, \quad (\text{A17})$$

where we used the condition $\tilde{\omega} = \omega_B$ since we consider only resonant scattering.

Radiation is described by two intensities $I_\perp(\omega, \mathbf{k})$ and $I_\parallel(\omega, \mathbf{k})$ in the two polarization states. They scatter with cross sections σ_{tot} that differ by the factor of $\tilde{\mu}^2$ (see Equations (A4) and (A6)). Substituting Equation (A4) to Equation (A16) and taking the sum over polarizations, one finds the net force exerted by I_\perp and I_\parallel ,

$$\frac{dP}{dt dV} = \int d\Omega \int d\omega \int dp \frac{(I_\perp + \tilde{\mu}^2 I_\parallel)}{\hbar\omega} n f_e(p) 2\pi^2 r_e c \delta(\tilde{\omega} - \omega_B) (1 - \beta\mu) \Delta P. \quad (\text{A18})$$

Integration over dp similar to that in Section A.2 gives

$$\frac{dP}{dt dV} = \int d\Omega \int_0^{\omega_B \sin \vartheta} d\omega 2\pi^2 r_e \frac{\omega_B}{\omega^2} (I_\perp + \tilde{\mu}^2 I_\parallel) n [\gamma_1 f_e(p_1) - \gamma_2 f_e(p_2)], \quad (\text{A19})$$

where $p_{1,2}(\omega, \vartheta)$ and $\gamma_{1,2}$ are given by Equations (A14) and (A12). The upper limit in the integral over ω takes into account that only photons with $\omega \leq \omega_B \sin \vartheta$ may be resonantly scattered (Section A.2). Equation (A19) is useful because it shows the contribution of each photon (ω, \mathbf{k}) (in the \perp or \parallel polarization state) to the drag force. It can be used even if the radiation intensity is not known in advance and needs to be found self-consistently with the plasma dynamics (Section 6).

An alternative way of simplifying Equation (A18) is to first integrate over ω , which gives

$$\frac{dP}{dt dV} = \int d\Omega \int dp 2\pi^2 r_e (I_\perp + \tilde{\mu}^2 I_\parallel) n f_e(p) \gamma(\mu - \beta), \quad (\text{A20})$$

where I_{\perp} and I_{\parallel} are evaluated at $\omega = \gamma^{-1}(1 - \beta\mu)^{-1}\omega_B$. Equation (A20) is convenient to use when the radiation intensity is known.

Note that Equations (A19) and (A20) are valid only where $B \ll B_Q$. Near the star, where the field is stronger, the drag force is modified (Baring et al. 2011; Beloborodov 2013). In this paper, we do not need the strong-field corrections, as radiative transfer occurs in the region of $B \ll B_Q$ (where the scattered photons avoid the quick conversion to e^{\pm} pairs); use of the full relativistic cross section would be an unnecessary complication.

B. OPTICALLY THIN OUTFLOW

Consider a magnetosphere that is optically thin to resonant scattering, so that intensity I is dominated by the unscattered radiation from the star. We will assume that the neutron star emits approximately blackbody radiation with the \perp polarization (the \perp photons dominate the surface radiation because they have a larger free path below the surface, e.g. Silant'ev & Iakovlev 1980). Then

$$I_{\perp} = \frac{\hbar\omega^3}{8\pi^3c^2[\exp(\hbar\omega/kT) - 1]}, \quad I_{\parallel} = 0, \quad (\text{B1})$$

and we deal with the outflow dynamics in the known radiation field. This case was studied in detail in previous work (e.g. Sturmer 1995).

B.1. Scattering rate for one particle

Consider an electron (or positron) located at r, θ and moving outward with Lorentz factor $\gamma = (1 - \beta^2)^{-1/2}$ along a magnetic field line. The number of photons scattered by the electron per unit time is

$$\dot{N}_{\text{sc}} = \int d\Omega \int d\omega \frac{I(\omega, \mathbf{n})}{\hbar\omega} \sigma_{\text{tot}} = \frac{2\pi^2 r_e c}{\gamma} \int \frac{I(\omega_{\text{res}}[\mathbf{n}], \mathbf{n})}{\hbar\omega_{\text{res}}} d\Omega, \quad (\text{B2})$$

where we substituted σ_{tot} (eq. A4). The resonant frequency depends on the photon direction, $\omega_{\text{res}} = \gamma^{-1}(1 - \beta \cdot \mathbf{n})^{-1}\omega_B$ where $\mathbf{n} = \mathbf{k}/k$ is the unit vector corresponding to $d\Omega$.

At large radii $r \gg R$ all photons at a given location \mathbf{r} have approximately the same direction $\mathbf{n} \parallel \mathbf{r}$. The angle between the stellar photons and the particle velocity, ϑ , is given by $\mu = \cos\vartheta \approx B_r/B$ (assuming $\vartheta > R/r$). Then integration over $d\Omega$ in Equation (B2) is reduced to multiplication by $\Delta\Omega \approx \pi(R/r)^2$, the solid angle subtended by the star when viewed from radius r . This gives,

$$\dot{N}_{\text{sc}} = \frac{2\pi^3 r_e c}{x^2 \gamma} \frac{I(\omega_{\text{res}})}{\hbar\omega_{\text{res}}} \quad \omega_{\text{res}} = \frac{\omega_B}{\gamma(1 - \beta\mu)}, \quad (\text{B3})$$

where $x = r/R$. It is instructive to write \dot{N}_{sc} in the following form,

$$\dot{N}_{\text{sc}} = \frac{\alpha \Theta^2 c}{4x^2 \gamma \lambda} \frac{g(y)}{y}, \quad (\text{B4})$$

where $\lambda = \hbar/m_e c$, $\Theta = kT/m_e c^2 \approx 10^{-3}$ and $g(y)$ is the dimensionless Planck function evaluated at the frequency $\omega_{\text{res}} = \gamma^{-1}(1 - \beta\mu)^{-1}\omega_B$,

$$g(y) = \frac{y^3}{e^y - 1}, \quad y = \frac{\hbar\omega_{\text{res}}}{kT} = \frac{b}{\gamma(1 - \beta\mu)\Theta}, \quad (\text{B5})$$

where $b = B/B_Q$.

B.2. Drag force exerted on one particle

The drag force applied by the central blackbody radiation to the electron is $\mathcal{F} = \dot{N}_{\text{sc}}\Delta P$ where ΔP is given by Equation (A17). This yields,

$$\mathcal{F}(\beta) = \frac{\alpha^2}{4x^2} \frac{m_e c^2}{r_e} \Theta^3 \gamma g(y) (\beta_{\star} - \beta), \quad (\text{B6})$$

where $\beta_{\star} = \mu$. Force \mathcal{F} vanishes if $\beta = \beta_{\star}$; in this case the radiation flux measured in the rest frame of the particle is perpendicular to \mathbf{B} and cannot accelerate or decelerate it. In a weakly twisted magnetosphere, the magnetic field in the outer corona is approximately dipole. Then the saturation velocity β_{\star} at a point r, θ (spherical coordinates) depends only on θ and is given by

$$\beta_{\star} = \mu = \frac{B_r}{B} = \frac{2 \cos \theta}{(1 + 3 \cos^2 \theta)^{1/2}}, \quad p_{\star} = \frac{2 \cos \theta}{\sin \theta}. \quad (\text{B7})$$

The radiative force always pushes the particle toward $p = p_{\star}$. This effect may be measured by the ‘‘drag coefficient,’’

$$\mathcal{D} \equiv \frac{r}{c} \frac{1}{p} \frac{dp}{dt}. \quad (\text{B8})$$

Consider an electron (or positron) with momentum $p \approx p_\star = \gamma_\star \beta_\star$. A small deviation $p - p_\star$ causes drag $\mathcal{D} \propto p - p_\star$, which may be written as

$$\mathcal{D} = \mathcal{D}_\star \left(1 - \frac{p}{p_\star}\right), \quad (\text{B9})$$

where

$$\mathcal{D}_\star = \frac{\alpha^2 R \Theta^3 g(y_\star)}{4 r_e x \gamma_\star^2} \approx \frac{4 \times 10^4 g(y_\star)}{x \gamma_\star^2} \left(\frac{kT}{0.5 \text{ keV}}\right)^3. \quad (\text{B10})$$

Here $y_\star = b\gamma_\star/\Theta$ corresponds to photons that are resonantly scattered by the electron with $p \approx p_\star$. The momentum p_\star is a strong attractor if $\mathcal{D}_\star \gg 1$. The value of \mathcal{D}_\star is sensitive to y_\star . In particular, in the equatorial plane, we have $\gamma_\star = 1$ and

$$y_\star \approx 1.6 \times 10^4 \left(\frac{B_{\text{pole}}}{10^{15} \text{ G}}\right) \left(\frac{kT}{0.5 \text{ keV}}\right)^{-1} \left(\frac{r}{R}\right)^{-3}, \quad (\theta = \pi/2), \quad (\text{B11})$$

where B_{pole} is the dipole field at the magnetic pole. The condition $\mathcal{D}_\star > 1$ corresponds to $y_\star \lesssim 20$. This implies that the e^\pm flow on magnetic field lines extending far from the star is stopped by the radiative drag in the equatorial plane. For typical magnetar parameters, the flow stops on field lines with $R_{\text{max}} \gtrsim 10R$.

B.3. Optical depth in the single-fluid approximation

The single-fluid flow has a distribution function $f_e(p') = \delta(p' - p)$ where $p(r, \theta)$ is the flow momentum. Then any photon of energy $\hbar\omega$ may only be scattered on the infinitesimally thin resonance surface defined by $\gamma(1 - \beta\mu)\omega = \omega_B$, where $\mu = \cos\vartheta$ describes the photon angle relative to the flow velocity. The optical depth of the resonant surface may be obtained from Equation (A9), which gives

$$\frac{d\tau}{ds} = 2\pi^2 r_e c n \xi (1 - \beta\mu) \delta(\tilde{\omega} - \omega_B), \quad (\text{B12})$$

where $\tilde{\omega} = \gamma(1 - \beta\mu)\omega$. One can use the identity,

$$\delta(\tilde{\omega} - \omega_B) = \sum_k \frac{\delta(s - s_k)}{\left|\frac{d}{ds}(\tilde{\omega} - \omega_B)\right|}. \quad (\text{B13})$$

The location s_k on the photon trajectory is where the photon crosses the resonant surface. Performing the integration over s along the photon trajectory, one finds the optical depth for one crossing of the resonant surface,

$$\tau = \frac{2\pi^2 r_e c n \xi (1 - \beta\mu)}{\left|\frac{d}{ds}(\tilde{\omega} - \omega_B)\right|}. \quad (\text{B14})$$

If we specialize to the case of central photons emitted by the neutron star with the \perp polarization,⁶ then $\xi = 1$ and $\mu = B_r/B$. For a moderately twisted dipole magnetosphere, the electric current density is given by $j \approx c\psi B/4\pi R_{\text{max}}$ (Beloborodov 2009), and

$$n = \mathcal{M} \frac{j}{ev} \approx \frac{\mathcal{M}\psi B}{4\pi e\beta R_{\text{max}}}. \quad (\text{B15})$$

Note that n is small on field lines with a large R_{max} , which implies a low optical depth near the axis; this fact was also emphasized by Thompson et al. (2002) who used a self-similar twist model.

The expression for the optical depth becomes particularly simple if the outflow has the equilibrium momentum $p = p_\star$. Then $d\tilde{\omega}/ds = 0$, i.e. $\tilde{\omega}$ remains constant along the radial ray through the outflow. This fact can be derived by noting that the Doppler factor $\gamma(1 - \beta\mu) = \gamma_\star^{-1}$ is a function of θ only — it does not depend on $s = r$ for the approximately dipole magnetosphere. It is also easy to see that $d\omega_B/ds = -3\omega_B/r$, and we find

$$\tau = \frac{\pi}{12} \mathcal{M}\psi \frac{\sin^4 \theta}{\cos \theta (1 + 3 \cos^2 \theta)^{1/2}}. \quad (\text{B16})$$

The single-fluid model with $p = p_\star$ may approximate the outflow only sufficiently close to the equatorial plane where $1 - \beta_\star \gtrsim \mathcal{M}^{-1}$. Nevertheless, the approximate Equation (B16) shows a general feature: the optical depth seen by the central photons is dramatically increased toward the equatorial plane ($\tau \propto \sec \theta$) and dramatically reduced toward the axis ($\tau \propto \sin^4 \theta$). As a result, a distant observer can see the unscattered radiation from the neutron-star surface when the line of sight is within a moderate angle $\theta < \pi/4$ from the polar axis. This feature becomes even more pronounced in the full radiative transfer problem where the relativistic outflow is decelerated by the reflected radiation from the outer corona. Then scattering of the central radiation is negligible in the entire relativistic zone of the outflow.

⁶ The neutron-star radiation is dominated by the \perp polarization (Silant'ev & Iakovlev 1980). In addition, for the outflow with the equilibrium momentum p_\star considered below, the scattering of \parallel

photons (even if they were included) would be suppressed. In the outflow rest frame, the photons move perpendicular to \mathbf{B} , and the resonant cross section for the \parallel polarization mode vanishes.

B.4. Drag force exerted on a plasma with a broad distribution function

Equation (B6) describes the drag force exerted by the central thermal radiation on a particle with a given momentum $p = \gamma\beta$. One can also consider a collection of particles with a momentum distribution $f_e(p)$ and derive the average force per particle $\bar{\mathcal{F}} = n^{-1}(dP/dVdt)$. Equation (A20) gives

$$\bar{\mathcal{F}} = \frac{r_e \hbar}{4c^2} \left(\frac{R}{r}\right)^2 \omega_B^3 \int_{-\infty}^{\infty} \frac{(\mu - \beta) f_e(p)}{\gamma^2 (1 - \beta\mu)^3 (\exp y - 1)} dp. \quad (\text{B17})$$

where y is given in Equation (B5). The same result is obtained by averaging the force \mathcal{F} given by Equation (B6), $\bar{\mathcal{F}} = \int \mathcal{F}(p) f_e(p) dp$.

Equation (B17) simplifies when the plasma is described by the waterbag distribution function f_e (Section 5.1); it leads to a straightforward calculation of the flow dynamics in the central radiation field. We use this simple outflow model as the first trial to initiate the iterations that converge to the solution shown in Figure 9. In the final solution, the drag exerted by the central radiation turns out negligible in the relativistic zone; instead, the outflow deceleration is controlled by the radiation streaming from the equatorial reflector, as discussed in Section 6. Then the force $\bar{\mathcal{F}}$ derived in this section may be of interest only in the non-relativistic zone.

C. NON-RESONANT SCATTERING

Non-resonant scattering is not limited by the resonance condition, and hence many more photons can participate in scattering, although with a smaller cross section. Below we discuss the effect of non-resonant scattering on the dynamics of e^\pm flow around magnetars.

Non-resonant scattering occurs mainly with photons in the Wien peak of the thermal radiation flowing directly from the neutron star, which dominates the photon density around the star. Relativistic particles see the thermal photons (of typical energy $E \sim 3kT$) blueshifted as $\tilde{E} = \gamma(1 - \beta\mu)E$ where $\mu = \cos\vartheta$ describes the photon direction relative to the particle velocity in the lab frame. Sufficiently far from the star (where $R^2/r^2 < 1 - B_r/B$) the radiation can be approximated as a narrow radial beam; then $\mu = B_r/B$. In general, μ is a function of the particle position r, θ, ϕ in the magnetosphere. For an approximately dipole field, $\mu = 2 \cos\theta (1 + 3 \cos^2\theta)^{-1/2}$ is a function of the polar angle θ only.

Magnetic field strongly affects the non-resonant scattering cross section if $\tilde{E} < \hbar\omega_B = bm_e c^2$. If the electron is relativistic, the target photons are aberrated in the electron rest frame, $\cos\tilde{\vartheta} = \tilde{\mu} = (\mu - \beta)/(1 - \beta\mu)$. In the limit $\beta \rightarrow 1$, even photons with the \parallel polarization have electric fields almost perpendicular to \mathbf{B} , which makes their scattering inefficient. For photons with $\tilde{E} \ll \hbar\omega_B$, the non-resonant scattering cross section is given by (e.g. Canuto et al. 1971)

$$\frac{\sigma_{\parallel}}{\sigma_{\text{T}}} \approx \left(\frac{\tilde{E}}{\hbar\omega_B}\right)^2 + \frac{\sin^2\tilde{\vartheta}}{2}, \quad \frac{\sigma_{\perp}}{\sigma_{\text{T}}} \approx \left(\frac{\tilde{E}}{\hbar\omega_B}\right)^2, \quad \tilde{E} \ll \hbar\omega_B. \quad (\text{C1})$$

We assume $\tilde{E} \ll m_e c^2$ and neglect Klein-Nishina corrections. Most of the radiation emitted by the neutron star has the \perp polarization.

The energy loss of the electron due to scattering is given by

$$\dot{E}_e = - \int d\Omega \int dE (1 - \beta\mu) \sigma(\tilde{E}) \frac{I(\mathbf{n}, E)}{E} (\overline{E'} - E), \quad (\text{C2})$$

where \mathbf{n} is the unit vector describing the photon direction in solid angle $d\Omega$, and $\overline{E'} = \gamma\tilde{E}$ is the mean expectation for the photon energy after scattering. This gives,

$$\dot{E}_e = - \int d\Omega \int dE (1 - \beta\mu) [\gamma^2(1 - \beta\mu) - 1] I(\mathbf{n}, E) \sigma(\tilde{E}) dE. \quad (\text{C3})$$

In the simplest case of Thomson scattering of isotropic radiation, averaging over random μ gives the standard result $\dot{E}_e = -(4/3)\sigma_{\text{T}} c U \gamma^2 \beta^2$, where U is the energy density of radiation. In our case, $\sigma < \sigma_{\text{T}}$, and the radiation field is not isotropic; far from the star it is better approximated as a central beam.

Using Equation (C3) one can show that non-resonant scattering makes a small contribution to the radiative drag compared with resonant scattering, and hence its inclusion in the calculation does not significantly change the outflow solution shown in Figure 9. Consider first the non-relativistic zone $p_+ < 1$. An upper bound on the non-resonant \dot{E}_e is obtained if we substitute into Equation (C3) $\sigma(\tilde{E}) = \sigma_{\text{T}}$ and $\mu = 0$. This gives,

$$\dot{E}_e = \sigma_{\text{T}} c p^2 U. \quad (\text{C4})$$

The drag coefficient due to non-resonant scattering is defined similar to Equation (B8). Using $U \approx L_{\text{th}}/4\pi r^2 c$ and $dp/dt = \dot{E}_e/\beta m_e c^2$, one obtains

$$\mathcal{D} \approx \frac{\sigma_{\text{T}} L_{\text{th}} \gamma}{4\pi r m_e c^3} \approx 0.2 L_{\text{th},35} r_6^{-1} \gamma \ll 1. \quad (\text{C5})$$

In the relativistic zone $p_+ > 1$, the upper bound given by Equation (C5) increases proportionally to γ and becomes useless, because it does not take into account the strong reduction of the scattering cross section below σ_T . In this zone, the outflow adjusts so that it can resonantly scatter photons with $E \sim 7kT$ and $\mu \sim -0.5$ (photons flowing from the equatorial reflector). This implies that the main targets for non-resonant scattering (photons flowing from the star with $E \sim 3kT$ and $\mu > 0$) have energies well below the resonance energy, $\bar{E} \sim (0.1 - 0.2)\hbar\omega_B$. Then the scattering cross section is strongly reduced below σ_T according to Equation (C1). When this reduction is taken into account, one obtains $\mathcal{D} < 1$.

REFERENCES

- Baring, M. G.; Wadiasingh, Z., & Gonthier, P. L. 2011, *ApJ*, 733, 61
- Beloborodov, A. M. 1998, *ApJ*, 496, L105
- Beloborodov, A. M. 2009, *ApJ*, 703, 1044
- Beloborodov, A. M. 2011a, in *High-Energy Emission from Pulsars and their Systems, Astrophysics and Space Science Proceedings*, 299 (Springer-Verlag), arXiv:1008.4388
- Beloborodov, A. M. 2011b, *ApJ*, 737, 68
- Beloborodov, A. M. 2013, *ApJ*, 762, 13
- Beloborodov, A. M., & Thompson, C. 2007, *ApJ*, 657, 967
- Berestetskii, V. B., Lifshitz, E. M., & Pitaevskii, L. P. 1982, *Quantum Electrodynamics*
- Camilo, F., et al. 2006, *Nature*, 442, 892
- Camilo, F., et al. 2007, *ApJ*, 666, L93
- Canuto, V., Lodenguai, J., & Ruderman, M. 1971, *Phys. Rev. D*, 3, 2303
- Cheng, A. F., & Ruderman, M. A. 1977, *ApJ*, 212, 800
- Daugherty, J. K., & Harding, A. K. 1986, *ApJ*, 309, 362
- Daugherty, J. K., & Harding, A. K. 1989, *ApJ*, 336, 861
- Daugherty, J. K., & Ventura, J. 1978, *Phys. Rev. D*, 18, 1053
- Fernández, R., & Davis, S. W. 2011, *ApJ*, 730, 131
- Fernández, R., & Thompson, C. 2007, *ApJ*, 660, 615
- Goldreich, P., & Julian, W. H. 1969, *ApJ*, 157, 869
- Harding, A. K., & Daugherty, J. K. 1991, *ApJ*, 374, 687
- Herold, H. 1979, *Phys. Rev. D*, 19, 2868
- Herold, H., Ruder, H., & Wunner, G. 1982, *A&A*, 115, 90
- Kardashev, N. S., Mitrofanov, I. G., & Novikov, I. D. 1984, *Sov. Astronomy*, 28, 651
- Krall, N. A., & Trivelpiece, A. W. 1973, *Principles of Plasma Physics*
- Medin, Z., & Lai, D. 2010, *MNRAS*, 406, 1379
- Lyubarskii, Y. E., & Petrova, S. A. 2000, *A&A*, 355, 406
- Nobili, L., Turolla, R., & Zane, S. 2008, *MNRAS*, 386, 1527
- Parfrey, K., Beloborodov, A. M., & Hui, L. 2012, 754, L12
- Parfrey, K., Beloborodov, A. M., & Hui, L. 2013, *ApJ*, in press (arXiv:1306.4335)
- Rea, N., Zane, S., Turolla, R., Lyutikov, M., & Götz, D. 2008, *ApJ*, 686, 1245
- Sturmer, S. J. 1995, *ApJ*, 446, 292
- Thompson, C. 2008a, *ApJ*, 688, 499
- Thompson, C. 2008b, *ApJ*, 688, 1258
- Thompson, C., & Beloborodov, A. M. 2005, *ApJ*, 634, 565
- Thompson, C., Lyutikov, M., & Kulkarni, S. R. 2002, *ApJ*, 574, 332
- Silant'ev, N. A., & Iakovlev, D. G. 1980, *Ap&SS*, 71, 45
- Sturrock, P. A. 1971, *ApJ*, 164, 529
- Ventura, J. 1979, *Phys. Rev. D*, 19, 1684
- Woods, P. M., & Thompson, C. 2006, in *Compact Stellar X-Ray Sources*, ed. W. H. G. Lewin & M. van der Klis (Cambridge: Cambridge Univ. Press), 547